



INSTITUT DE FRANCE  
Académie des sciences

# *Comptes Rendus*

---

## *Géoscience*

### *Sciences de la Planète*

Han Liu, Zhangji Zhao, Qi Zhou, Ruoxia Chen, Kai Yang, Zhe Wang,  
Longwen Tang and Mathieu Bauchy

#### **Challenges and opportunities in atomistic simulations of glasses: a review**

Volume 354, Special Issue S1 (2022), p. 35-78


Published online: 2 May 2022

Issue date: 29 May 2023

<https://doi.org/10.5802/crgeos.116>

**Part of Special Issue:** Glass, an ubiquitous material

**Guest editor:** Daniel Neuville (Université de Paris, Institut de physique du globe de Paris, CNRS)

 This article is licensed under the  
CREATIVE COMMONS ATTRIBUTION 4.0 INTERNATIONAL LICENSE.  
<http://creativecommons.org/licenses/by/4.0/>



*Les Comptes Rendus. Géoscience — Sciences de la Planète sont membres du  
Centre Mersenne pour l'édition scientifique ouverte*

[www.centre-mersenne.org](http://www.centre-mersenne.org)

e-ISSN : 1778-7025



---

Glass, an ubiquitous material / *Le verre, un matériau omniprésent*

# Challenges and opportunities in atomistic simulations of glasses: a review

*Défis et opportunités en simulations atomiques de verres :  
une revue*

Han Liu<sup>✉</sup><sup>a</sup>, Zhangji Zhao<sup>a</sup>, Qi Zhou<sup>a</sup>, Ruoxia Chen<sup>a</sup>, Kai Yang<sup>a</sup>, Zhe Wang<sup>a</sup>,  
Longwen Tang<sup>a</sup> and Mathieu Bauchy<sup>✉\*</sup><sup>a</sup>

<sup>a</sup> Physics of Amorphous and Inorganic Solids Laboratory (PARISlab), Department of Civil and Environmental Engineering, University of California, Los Angeles, CA 90095, USA

*E-mails:* happyliu@ucla.edu (H. Liu), zzhao13@ucla.edu (Z. Zhao), qi1197@ucla.edu (Q. Zhou), ruoxia@g.ucla.edu (R. Chen), tzyk4707@outlook.com (K. Yang), franciscowang@ucla.edu (Z. Wang), whulongwen@gmail.com (L. Tang), bauchy@ucla.edu (M. Bauchy)

**Abstract.** Atomistic modeling and simulations have been pivotal in our understanding of the glassy state. Indeed, atomistic modeling offers direct access to the structure and dynamics of atoms in glasses—which is typically hidden from conventional experiments. Simulations also offer a more economical, faster alternative to systematic experiments to decode composition-property relationships and accelerate the discovery of new glasses with desirable properties and functionalities. However, the atomistic modeling of glasses remains plagued by a series of challenges, e.g., high computational cost, limited accessible timescale, lack of accurate interatomic forcefields, etc. These challenges often result in the existence of discrepancies between simulation and experimental data, thereby limiting the predictive power of atomistic modeling. Here, we review recent accomplishments and remaining challenges facing the atomistic modeling of glasses. We discuss future opportunities offered by the seamless integration of simulations, knowledge, experiments, and machine learning in advancing glass modeling to a new era.

**Résumé.** La modélisation et simulations atomiques ont joué un rôle important pour notre connaissance de l'état vitreux. En effet, la modélisation atomique offre un accès direct à la structure et dynamique des atomes dans les verres — qui n'est typiquement pas accessible par les techniques expérimentales classiques. Les simulations offrent également une alternative économique et rapide aux expériences systématiques pour décoder les relations composition-propriétés et accélérer la découverte de nouveaux verres offrant des propriétés et fonctionnalités de choix. Cependant, la modélisation atomique des verres reste limitée par une série de défis, par exemple, le coût de calcul élevé, l'échelle de temps accessible limitée, le manque de champs de force interatomiques précis, etc. Ces défis induisent souvent l'existence de divergences entre les résultats simulés et expérimentaux, ce qui limite le pouvoir prédictif de la modélisation atomistique. Dans cette contribution, nous passons en revue les

---

\* Corresponding author.

récents progrès et les défis restants auxquels est confrontée la modélisation atomistique des verres. Nous discutons les opportunités futures offertes par les intégrations de simulations, connaissances, données expérimentales et d'intelligence artificielle pour faire avancer la modélisation du verre vers une nouvelle ère.

**Keywords.** Molecular dynamics, Interatomic forcefield, Reserve Monte Carlo, Machine learning, Accelerated simulation, Differentiable programming, Inverse design.

**Mots-clés.** dynamique moléculaire, champ de force interatomique, Monte Carlo, machine learning, simulation accélérée, programmation différentiable, design inverse.

*Published online: 2 May 2022, Issue date: 29 May 2023*

## 1. Introduction

As out-of-equilibrium phases, glasses exhibit a complex disordered atomistic structure that can virtually accommodate the entire periodic table [Mauro, 2018, Musgraves *et al.*, 2019, Zanotto and Coutinho, 2004]. This structural complexity has historically limited our ability to unveil structure–property relationships in glasses [Bapst *et al.*, 2020, Tanaka *et al.*, 2019, 2010], but, in turn, offers a vast design space to discover new glasses with unusual properties [Liu *et al.*, 2019d, Onbaşlı *et al.*, 2018, Ravinder *et al.*, 2020]. Although different experimental protocols have been developed to investigate the nature of the linkages between glass composition, structure, and properties [Almeida and Santos, 2015, Kamitsos, 2015, Salmon and Zeidler, 2015, Youngman, 2018], they yield a series of structural fingerprints that are experimentally accessible—e.g., pair distribution function (PDF) computed by diffraction experiments or coordination numbers accessed by nuclear magnetic resonance (NMR) [Fischer *et al.*, 2005, Kroeker, 2015, Wright, 1988, Youngman, 2018]—rather than offering a direct access to the three-dimensional atomic structure itself [Affatigato, 2015, Greaves and Sen, 2007, Huang *et al.*, 2013, Yang *et al.*, 2021, Zhou *et al.*, 2021]. In that regard, atomistic simulations have become a routine tool to easily access the atomistic structure of glasses [Bauchy, 2019, Du, 2019, Pedone, 2009]—which is otherwise invisible from conventional experiments [Pandey *et al.*, 2016b,a]—and to decipher the physical nature of the linkages between glass structure and properties [Binder and Kob, 2011, Massobrio, 2015, Onbaşlı and Mauro, 2020]. Atomistic simulations of glasses can be broadly divided into two different families, namely, knowledge-based and data-based.

### 1.1. *Physical-knowledge-based simulations*

As a primary goal, atomistic simulations aim to reveal the atomistic structure of glasses [Mauro *et al.*, 2016, Takada, 2021]. This can be achieved by explicitly simulating the time-dependent formation process of glasses—e.g., melt-quenching [Debenedetti and Stillinger, 2001], sol–gel transition [Du *et al.*, 2018], vapor deposition [Wang *et al.*, 2020], irradiation [Krishnan *et al.*, 2017a,b], or annealing [Grigoriev *et al.*, 2016]. Such simulations rely on our knowledge of the physics governing the interaction between atoms, i.e., the interatomic forcefields (see Figure 1) [Massobrio, 2015, Mauro *et al.*, 2016, Onbaşlı and Mauro, 2020]. In detail, starting from the sole knowledge of first-principles electron interactions [Hohenberg and Kohn, 1964, Kohn and Sham, 1965], one can compute the interatomic interactions acting in a glass system [Boero *et al.*, 2015, Hafner, 2008]. In turn, this interatomic forcefield drives the motions of the atoms as per Newton's law of motion—which is the basic principle behind molecular dynamics (MD) simulations [Alder and Wainwright, 1959, Takada, 2021]. In other words, MD simulations predict the spontaneous motions of the atoms in glasses (or liquids) [Durandurdu and Drabold, 2002, Micoulaut *et al.*, 2013]. However, since MD simulations are generally limited to short timescales (typically up to a few nanoseconds) [Lane, 2015], it is intrinsically unable to match experimental timescale (up to days) [Li *et al.*, 2017]. In particular, as the most common method to prepare a glass [Mauro and Zanotto, 2014], the melt-quenching process consists in melting a liquid that is then cooling into a glass. However, the cooling rates that are accessible to MD simulations ( $10^{14}$ – $10^9$  K/s) are orders of magnitude larger than those experienced in conventional experiments ( $10^2$ – $10^0$  K/s) [Li *et al.*, 2017, Vollmayr *et al.*, 1996a,b]. Note that, although the short timescale accessible

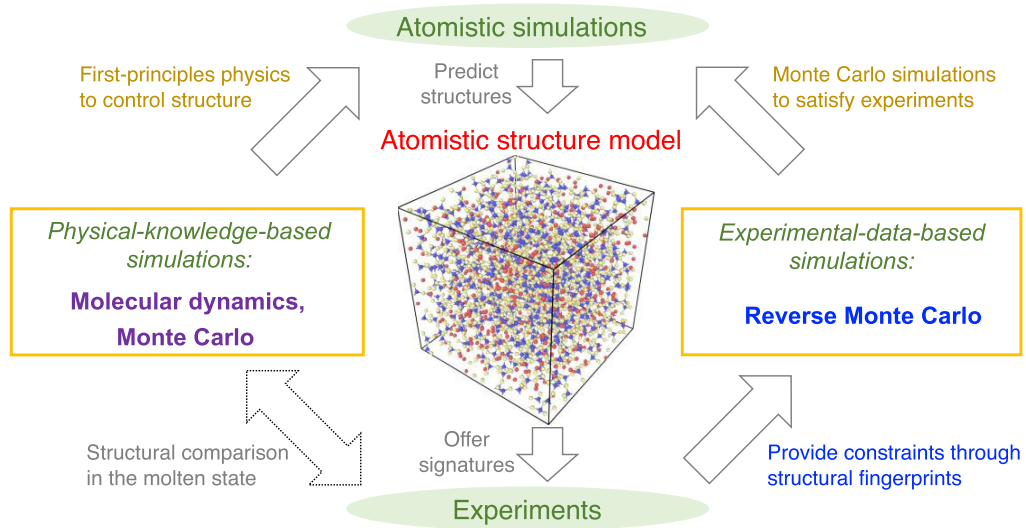


**Figure 1.** Schematic illustrating the atomistic simulation of glasses through (i) physical-knowledge-based simulations, e.g., molecular dynamics (MD) simulations [Soules, 1990], and (ii) experimental-data-based simulations, e.g., reverse Monte Carlo (RMC) simulations [McGreevy, 2001]. Simulations offer a direct access to the atomistic structure of glasses that can be validated by experiments, while, in turn, experiments can offer some fingerprints of the atomistic structure that can be used as simulation constraints. Note that, despite the pronounced difference of timescale between experiments and MD simulations, a direct comparison between MD and experimental data is possible for melts—since the structure and properties of equilibrium liquids and metastable-equilibrium supercooled liquids do not depend on their thermal history [Le Losq *et al.*, 2017].

to MD simulations challenges the comparison between glasses prepared by melt-quenching experiments and MD simulations, it should be pointed out that direct comparisons are possible when the simulated system is at equilibrium (liquid) or metastable equilibrium (supercooled liquid) since the structure and properties of such systems do not depend on their thermal history (see Figure 1) [Le Losq *et al.*, 2017].

To overcome the short timescale accessible to MD simulations [Li *et al.*, 2017], various simulation techniques have been proposed to accelerate the exploration of a glass’s potential energy landscape (PEL)—which represents the topography of the potential energy of a system as a function of its atom positions [Debenedetti and Stillinger, 2001, Lacks, 2001, Lacks and Osborne, 2004]. Although MD simulates the real, spontaneous evolution of the system within its PEL, its limited timescale typically prevents large energy barriers to be overcome [Yu *et al.*, 2017b, 2015]. In contrast, accelerated simulation techniques tend to

push systems across energy barriers to accelerate their dynamics, but such accelerated dynamics may not always match the spontaneous dynamics of the atoms [Bauchy *et al.*, 2017, Fullerton and Berthier, 2020, Liu *et al.*, 2019a]. As one of the most simple sampling technique, energy-based Monte Carlo (MC) simulations aim to explore the PEL of a glass by performing a series of random “moves” (e.g., by displacing a randomly selected atom) [Allen and Tildesley, 2017, Utz *et al.*, 2000] so as to discover lower-energy states in the PEL [Arceri *et al.*, 2020, Vollmayr-Lee *et al.*, 2013, Welch *et al.*, 2013]. However, since MC moves do not necessarily reproduce the spontaneous dynamics of a glass as it relaxes toward lower-energy states, it is not guaranteed that the simulated glass matches that formed by experiments [Berthier and Ediger, 2020].

## 1.2. Experimental-data-based simulations

To overcome the limitations of simulations based on physical knowledge [Berthier and Ediger, 2020, Li *et al.*, 2017, Wright, 2020], simulations based on experimental data—e.g., reverse Monte Carlo (RMC) simulations [Biswas *et al.*, 2004, Keen and McGreevy, 1990] or empirical potential structure refinement (EPSR) simulations [Nienhuis *et al.*, 2021, Soper, 2005, Weigel *et al.*, 2008]—have been proposed to invert experimental data (i.e., structural signatures of the real underlying atomic structure) into a three-dimensional atomic structure. In detail, RMC simulations adopt an MC search algorithm [Allen and Tildesley, 2017] wherein a series of MC moves (e.g., random displacement of atoms) is performed so as to eventually obtain a glass structure that satisfies the structural constraints provided by experiments [McGreevy, 2001, McGreevy and Pusztai, 1988]. In the same spirit, EPSR simulations reduce the difference between simulation and experimental data by iteratively tuning the coefficients of a predefined empirical potential until the structure simulated by MD matches experiments. As compared to RMC, EPSR simulations tend to yield more realistic structures (which satisfy some basic stability constraints imposed by the empirical potential). However, the accuracy of EPSR simulations can be limited by the choice of the analytical form that is adopted for the empirical potential [Nienhuis *et al.*, 2021, Soper, 2005, Weigel *et al.*, 2008].

Figure 1 shows a schematic illustrating the interactions between experiments and simulations. On the one hand, experiments can extract various signatures (e.g., PDF computed by diffraction experiments [Wright, 1988]) of the atomic structure of glasses [Affatigato, 2015], which can be used to validate knowledge-based simulations. On the other hand, RMC simulations can utilize these structural signatures as constraints to “inversely” construct an atomistic structure that satisfies available experimental data [McGreevy, 2001]. It is notable that simulations based on experimental data effectively bypass any explicit glass formation process (e.g., melt-quenching) and, hence, are not affected by the limited timescale accessible to atomistic simulations. However, such simulations cannot offer any physical insights in the dynamics of the atoms in a glass [Bot-taro and Lindorff-Larsen, 2018, Pandey *et al.*, 2016b,

Yu *et al.*, 2015].

In the following, we briefly review the state of the art in atomistic simulations of glasses in Section 2. The present challenges facing these simulations are discussed in Section 3. To address these challenges, we then highlight several new opportunities to advance the atomistic modeling of glasses in Section 4. Finally, we offer some concluding remarks in Section 5.

## 2. Overview of the state of the art in atomistic simulations of glasses

### 2.1. Basic principles of atomistic simulations of glasses

#### 2.1.1. Newton’s law of motion

As an alternative classification, simulations can be broadly divided in terms of their description of the atomic motion. Namely, (i) MD simulations offer a direct description of the spontaneous dynamics of the atoms as per Newton’s law of motion, whereas (ii) other types of simulations (e.g., MC or RMC simulations) simply aim to construct an atomic structure based on a target objective (e.g., minimizing energy and maximizing agreement with experiments) without any explicit description of the dynamics of the atoms [Allen and Tildesley, 2017, Takada, 2021]. MD simulations predict the motion of the atoms that is predicted by Newton’s law of motion (see Figure 2a) [Alder and Wainwright, 1959, Pedone, 2009]. This requires the knowledge of the interatomic forcefield, that is, the force experienced by each atom. Such forces can comprise radial 2-body interactions, angular 3-body interactions, and/or many-body interactions [Daw and Baskes, 1983, Stillinger and Weber, 1985] and play a key role in predicting atom trajectories [Du, 2015, Huang and Kieffer, 2015]. In practice, the interatomic forcefield can be accurately computed using first-principles electron-level methods (e.g., *ab initio* MD simulation [Boero *et al.*, 2015, Hafner, 2008]) or can be approximately estimated by some empirical functions (i.e., classical MD simulation [Carré *et al.*, 2016, 2008]). More technical details are provided in Sections 2.3 to 2.6.

#### 2.1.2. Minimum search in a cost function landscape

Unlike MD simulations [Massobrio, 2015], RMC [McGreevy, 2001], energy-based MC [Allen and

Tildesley, 2017, Liu *et al.*, 2019f, Utz *et al.*, 2000], or energy minimization based on gradient descent [Bitzek *et al.*, 2006, Shewchuk, 1994] do not follow Newton’s law of motion. Rather, these approaches rely on exploring and finding the minimum position of a given “cost landscape” (e.g., potential energy for MC and energy minimization, or a loss difference between simulated and experimental fingerprints for RMC) via a series of structural modifications (e.g., displacing atoms) [McGreevy, 2001, Takada, 2021]. For instance, Figure 2b illustrates the principle behind energy-based MC simulations [Allen and Tildesley, 2017], wherein the MC simulation searches the global minimum within the PEL by performing a series of tentative MC moves. Each move is either accepted or rejected according to a given acceptance probability defined in the MC algorithm (see Section 2.2) [Liu *et al.*, 2019f, McGreevy and Pusztai, 1988]. In contrast to MD simulations wherein large energy barriers are unlikely to be overcome [Debenedetti and Stillinger, 2001, Liu *et al.*, 2019a], simulations based on sampling a PEL can “accelerate” atomic motion to (i) jump over energy barriers and (ii) move toward the minimum energy state [Utz *et al.*, 2000, Yu *et al.*, 2015], which corresponds to the most stable energy state that the glass relaxes toward upon aging/relaxation [Welch *et al.*, 2013]. Note that the landscape to explore (i.e., the function to minimize) is not always the potential energy [Debenedetti and Stillinger, 2001, Tang *et al.*, 2021], but, rather, can take the form of any function, e.g., a loss function capturing the structural difference between simulated and experimental glass in the case of RMC simulations [McGreevy, 2001]. More technical details on RMC are provided in Section 2.2.

## 2.2. Reverse Monte Carlo (RMC) simulations

### 2.2.1. Cost function

RMC simulations rely on the MC search algorithm to generate an atomistic structure satisfying experimental structural constraints (i.e., measured structural fingerprints) [Keen and McGreevy, 1990, McGreevy, 2001, McGreevy and Pusztai, 1988]. In detail, the simulation searches for the global minimum in a cost function landscape as a function of the system’s atom positions (see upper panel in Figure 3a)

by performing a series of random atomic displacements (“MC move”, see lower panel in Figure 3a) [McGreevy, 2001]. Here, the cost function  $R_\chi$  is defined as the magnitude of difference between a simulation result and its experimental reference—often, the simulated and experimental PDFs  $g(r)$ , formulated as follows [Wright, 1993, Zhou *et al.*, 2020]:

$$R_\chi = \sqrt{\frac{\sum_r [g^{\text{exp}}(r) - g^{\text{sim}}(r)]^2}{\sum_r [g^{\text{exp}}(r)]^2}}, \quad (1)$$

where the superscript of  $g(r)$  denotes experiment (exp) or simulation (sim).

### 2.2.2. Acceptance rate of RMC search

In analogy to the conventional energy-based Metropolis MC algorithm [Allen and Tildesley, 2017], the acceptance probability  $P$  of each MC move can be expressed as [Zhou *et al.*, 2020]:

$$P = \begin{cases} 1 & \text{if } R_\chi^{\text{new}} \leq R_\chi^{\text{old}} \\ \exp\left[-\frac{R_\chi^{\text{new}^2} - R_\chi^{\text{old}^2}}{T_\chi}\right] & \text{if } R_\chi^{\text{new}} > R_\chi^{\text{old}} \end{cases} \quad (2)$$

where  $T_\chi$  plays the role of a (unit less) “effective temperature” that controls the probability of acceptance [Liu *et al.*, 2019f, Utz *et al.*, 2000], and  $R_\chi^{\text{old}}$  and  $R_\chi^{\text{new}}$  are the values of the cost function  $R_\chi$  (analogous to the role of the energy in energy-based MC [Utz *et al.*, 2000]) at the current and next MC step, respectively. Note that, in contrast, for instance, to a steepest descent minimization, a move that increases the value of the cost function still has a nonzero probability of acceptance in this algorithm. This makes it possible to overcome some barriers in the landscape during sampling—so that the system does not remain stuck in local minima. The RMC simulation proceeds until the cost function does not exhibit any noticeable decay upon additional MC moves, that is, until the cost function exhibits a plateau.

### 2.2.3. Structural match to experimental data

RMC simulations generally yield atomistic structures that exhibit an excellent agreement with the experimental data that are used to define the cost function (e.g., PDF) [Keen and McGreevy, 1990], which is not surprising since RMC solely aims to minimize the difference between simulated and experimental structural data. Figure 3b shows the evolution of the cost function  $R_\chi$  as a function of the number of MC search steps during the RMC simulation of a sodium silicate glass  $((\text{Na}_2\text{O})_{30}(\text{SiO}_2)_{70})$  [Zhou *et al.*, 2020],

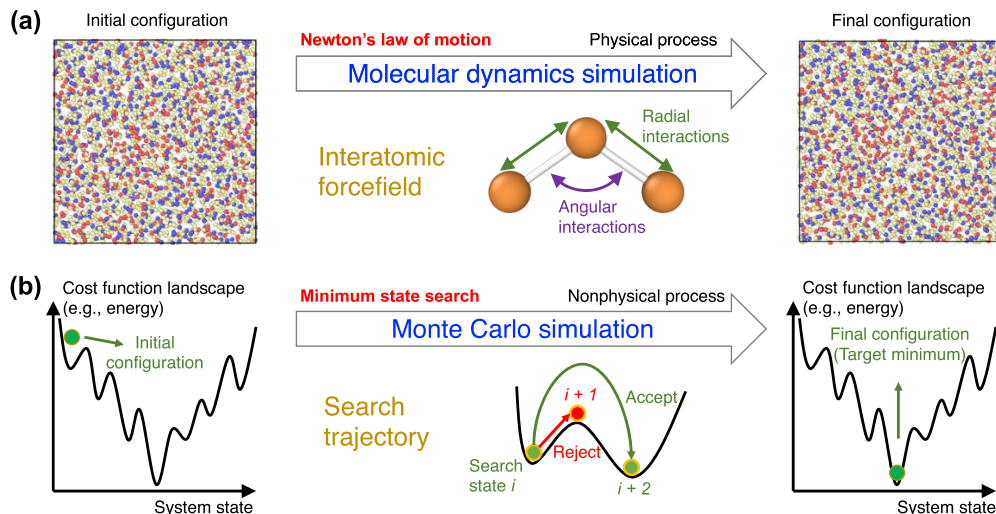


**Figure 2.** (a) Illustration of a molecular dynamics (MD) simulation of a glass system, wherein, starting from an initial configuration, the motion of the atoms is determined based on the interatomic interactions following Newton’s law of motion. (b) Illustration of a Monte Carlo (MC) simulation, wherein an MC search algorithm (e.g., energy-based Metropolis algorithm [Allen and Tildesley, 2017]) is used to find the minimum state (e.g., minimum energy) of a glass system within a cost function landscape—e.g., potential energy landscape (PEL), namely, a system’s potential energy as a function of its atom positions [Lacks, 2001]. The landscape is sampled by performing a series of MC moves (e.g., random displacement of an atom) [Takada, 2021].

wherein the cost function is defined based on the neutron PDF. As expected,  $R_\chi$  gradually decreases and, finally, the simulation generates an atomistic structure that exhibits an excellent match with experimental data. Further, Figure 3c shows the PDF  $g(r)$  computed both at the start and end of the RMC simulation. As expected, the final configuration exhibits an excellent agreement with the experimental reference, i.e., the measured  $g(r)$  [McGreevy, 2001, Pandey et al., 2015, Zhou et al., 2020].

RMC simulations have successfully been used to reveal the structure of a variety of glasses or amorphous solids, especially in the case of systems that are too complex to be simulated by MD or for which no reliable empirical forcefield is available. Example of simulated systems include nuclear waste glasses [Bouty et al., 2014], metal-organic frameworks (MOFs) [Beake et al., 2013, Gaillac et al., 2017], calcium carbonate [Fernandez-Martinez et al., 2013, Goodwin et al., 2010], etc. Overall, RMC simulations offer a powerful tool to model glasses when accurate experimental data are available [Playford et al., 2014].

### 2.3. Molecular dynamics (MD) simulations

MD simulations rely on interatomic forcefields to predict the trajectory of the atoms according to Newton’s law of motion [Alder and Wainwright, 1960, 1959, Rahman and Stillinger, 1971, Stillinger and Rahman, 1974]. Despite their short timescale [Li et al., 2017], MD simulations reproduce the formation process of glasses (e.g., melt quenching process under high cooling rate) to form the atomistic structure of a glass [Bauchy, 2014, Micoulaut et al., 2013]. In this section, we provide some general guidelines to implement MD simulations of glasses.

#### 2.3.1. Numerical algorithm

The algorithm of MD simulations consists of a loop of four successive steps (see Figure 4a) [Allen and Tildesley, 2017, Takada, 2021], namely, (i) computing the system’s potential energy  $U(\{r_i\})$  by summing up all interatomic interactions for the current atom positions  $\{r_i\}$ , (ii) calculating the resultant force  $\{F_i\}$  experienced by each atom  $i$  via energy differentiation (i.e.,  $F_i = -\partial U / \partial r_i$ ), (iii) obtaining each atom’s

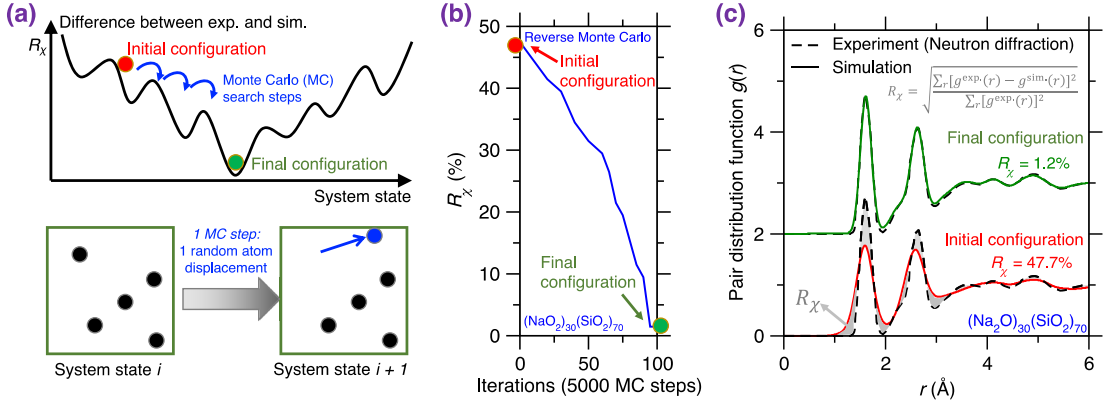


**Figure 3.** (a) Illustration of a Reverse Monte Carlo (RMC) simulation based on the Monte Carlo (MC) search algorithm to find the glass configuration that minimizes a given cost function [McGreevy, 2001], where the cost function  $R_\chi$  is defined as the magnitude of difference between a simulation result and its experimentally measured reference. Each MC search step consists of randomly displacing a randomly selected atom. (b) Evolution of the cost function  $R_\chi$  as a function of the number of MC search steps during an RMC simulation of a sodium silicate glass  $((\text{Na}_2\text{O})_{30}(\text{SiO}_2)_{70})$  [Zhou et al., 2020].  $R_\chi$  is defined herein as the magnitude of difference between the simulated and experimental neutron PDF  $g(r)$  (see (1)). (c) Comparison between the simulated  $g(r)$  and its experimental reference both at the start and end of the RMC simulation [Zhou et al., 2020]. The gray area represents the difference (i.e.,  $R_\chi$ ) between the experimental and simulated PDF.

acceleration  $\{a_i\}$  from  $\{F_i\}$  as per Newton's law of motion, that is,  $a_i = F_i/m_i$ , where  $m_i$  is the mass of atom  $i$ , and finally, (iv) updating the atom positions and velocities after a small, fixed timestep via numerical integration (e.g., Verlet or leapfrog algorithm) [Allen and Tildesley, 2017]. Eventually, this four-step loop yields the position of the atom as a function of time, that is, the trajectory of each atom.

It should be pointed out that the accuracy of an MD simulation depends on (i) the realistic nature of the initial configuration (i.e., initial positions and velocities), (ii) the value of the integration timestep, and, importantly, (iii) the accuracy of the interatomic potential energy. First, in the case of the glasses, the initial configuration is usually constructed by randomly placing some atoms in a cubic box while ensuring the absence of any unrealistic overlap (see below). The configuration is then relaxed at elevated temperature until the system loses the memory of its initial configuration. At this point, the outcome of the simulation does not depend any longer on how realistic the initial configuration was. Second, the integration timestep needs to be small enough ( $\sim 1$  fs)

to ensure the accuracy of the numerical integration. In practice, one can check that the timestep is small enough by ensuring the conservation of the system's total energy and linear/angular momentum during a simulated dynamics in the microcanonical ( $NVE$ ) ensemble [Grubmüller et al., 1991, Levesque and Verlet, 1993, Omelyan et al., 2002]). Third, if the integration timestep is small enough, the accuracy of the MD simulation primarily depends on that of the underlying potential energy (see Figure 4a) [Du, 2015, Huang and Kieffer, 2015].

Relying on the most fundamental quantum mechanics describing electron interactions (i.e., first-principles calculation of electron interactions) [Hohenberg and Kohn, 1964, Kohn and Sham, 1965], the interatomic interactions can be accurately computed by conducting first-principles MD simulation (i.e., *ab initio* MD simulation [Boero et al., 2015], see Section 2.4). Such simulations are computationally expensive but can be used to validate or inform classical MD simulations relying on simplified, empirical potential energy functionals (see Section 2.5) [Carré et al., 2008].



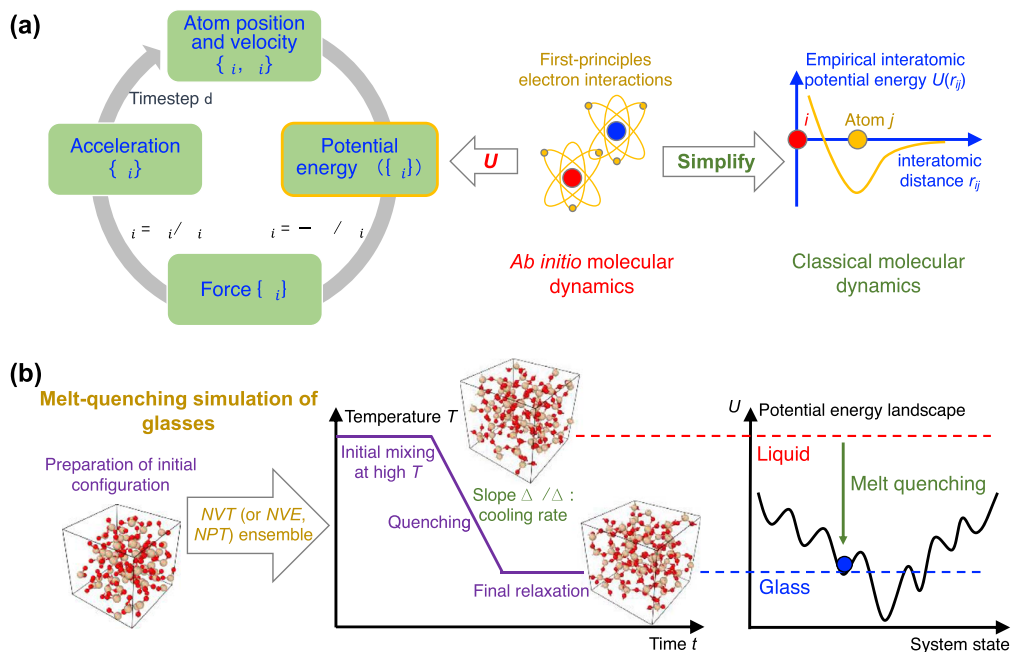


**Figure 4.** (a) Numerical algorithm of molecular dynamics (MD) simulation, which consists of an iterative succession of four computational steps (see text for details) [Takada, 2021]. *Ab initio* MD computes the potential energy  $U(\{r_i\})$  based on first-principles electronic interactions [Boero et al., 2015], whereas, in classical MD, the interatomic interaction is approximately estimated by some empirical functionals [Huang and Kieffer, 2015]. (b) Schematic illustrating a melt-quenching simulation for glassy silica. After an initial  $\text{SiO}_2$  configuration is prepared, the system is melted under high temperature in the  $NVT$  ensemble (or other ensembles, e.g.,  $NPT$  ensemble), quenched with a given cooling rate to a low temperature, and finally relaxed at this temperature [Carré et al., 2016]. From the viewpoint of the potential energy landscape (PEL) [Wilkinson and Mauro, 2021], starting from the high-energy, ergodic liquid state, the system gradually evolves to some nonergodic, low-energy states and finally gets trapped in a local minimum corresponding to a glassy state [Debenedetti and Stillinger, 2001, Goldstein, 1969].

### 2.3.2. Thermodynamical ensembles

A direct numerical solution of Newton's law of motion yields the microcanonical  $NVE$  dynamics of the  $N$  atoms, that is, wherein the total energy and volume of the system are conserved. However, the  $NVE$  ensemble does not always mimic experimental conditions. In practice, a system can either be isolated from the rest of the universe (i.e., presenting a constant energy) or be in contact with a thermostat (wherein the thermostat can provide or receive energy so as to fix the temperature  $T$  of the system). The volume  $V$  of the system can also either be fixed or variable based on the pressure  $P$  imposed by a barostat. As such, the most common thermodynamic ensembles used

in MD simulations are the microcanonical ( $NVE$ ), canonical ( $NVT$ ), and isothermal-isobaric ( $NPT$ ) ensembles [Du, 2019, Leach, 2001]. Simulating the motion of the atoms in a non- $NVE$  ensemble (e.g.,  $NVT$  or  $NPT$ ) requires slight modification to the constitutive equations used to calculate the acceleration of each atom [Allen and Tildesley, 2017, Du, 2019]. On the one hand, simulating a constant-temperature dynamics requires the use of a thermostat-based MD algorithm (e.g., Nosé-Hoover thermostat [Hoover, 1985, Nosé, 1984a,b]) to adjust on-the-fly the atomic velocities so as to achieve a target temperature [Andersen, 1980, Martyna et al., 1996]. On the other hand, simulating a constant-pressure dynamics involves the use of a barostat-based MD algorithm

[Allen and Tildesley, 2017, Leach, 2001] (e.g., Nose–Hoover barostat [Martyna *et al.*, 1992]) to adjust on-the-fly the system’s volume so as to achieve a target pressure (or state of stress) [Martyna *et al.*, 1996, Tuckerman *et al.*, 2006]. More details can be found in Allen and Tildesley [2017], Leach [2001].

### 2.3.3. *Melt-quenching simulations*

The most common method used in MD to prepare a glass consists in mimicking the experimental melt-quenching process [Soules, 1990]. The melt-quenching process is detailed in the following and illustrated by Figure 4b for the case of a silica glass [Carré *et al.*, 2008, Liu *et al.*, 2019e].

First, an initial configuration must be created. To this end, one option is to start with a crystalline configuration (e.g.,  $\alpha$ -quartz in the case of a silica glass). However, this is often not the preferred option as (i) there might not exist a crystal with the same composition as that of the target glass, (ii) the crystal might have a very different density from that of the glass, (iii) the shape of the unit cell of the crystal (e.g., triclinic unit cell) might result in an unnecessarily complicated simulation box geometry, and (iv) melting the initial crystalline structure might require high temperature and/or long simulation time. As an alternative—often preferred—option, the initial configuration can be prepared by randomly placing atoms or molecules (e.g.,  $\text{SiO}_2$  molecules in the case of a silica glass) into a cubic simulation box with periodic boundary conditions (PBC) [Leach, 2001]. The box size can either be fixed so as to match the experimental density of the glass (if when the quenching is performed in the *NVT* ensemble) or to an arbitrary value (if the quenching is performed in the *NPT* ensemble). Note that, when creating the initial configuration, care must be taken to avoid any unrealistic atom overlap that might cause spurious fast atom motions at the beginning of the simulation [Martínez *et al.*, 2009]. This can be achieved by imposing a cutoff threshold when randomly placing the atoms, e.g., by ensuring that the distance between a pair of atoms is never lower than the sum of their radii or that a pair of cations (or anions) are never close to each other.

Second, the initial configuration must be melted at high temperature so as to fully lose the memory of the initial configuration. The choice of the melting temperature depends on the type of glass that is

considered. On the one hand, the temperature must be high enough to ensure that the atoms move fast enough to “reset” the initial configuration or fully melt the initial crystal. On the other hand, a temperature that is too high might induce some spurious instabilities (e.g., due to the “Buckingham catastrophe” [Carré *et al.*, 2008] or if the system approaches the vaporization point) and increase the length of the simulation (since, at fixed cooling rate, a higher initial temperature increases the duration of cooling). The fact that the initial melting is long enough to ensure that the system has lost the memory of its initial configuration can be checked by computing the intermediate scattering function (ISF) or, as an approximate rule of thumb, by ensuring that the atoms have, on average, diffused by at least half of the simulation box.

Third, the melt is quenched to the glassy state by decreasing temperature. This is typically achieved by linearly decreasing temperature over time, while other more complicated thermal routes can be considered (e.g., nonconstant cooling rate or step-by-step cooling). The cooling process can either be performed in the *NVT* or *NPT* ensemble. The *NPT* ensemble is usually desirable as it mimics the experimental synthesis of glass (i.e., wherein the melt is quenched under atmospheric pressure). In turn, the *NVT* ensemble can yield some spurious effects as, since density is fixed, the pressure changes as a function of temperature. As a result, when using the *NVT* ensemble during cooling, the glass tends to “freeze” under positive (compressive) pressure at the glass transition temperature, which can impact the resulting structure. However, some interatomic force-fields are unable to yield the correct final glass density, so that using the *NVT* ensemble and fixing the volume to achieve the experimental glass density might, in some cases, be necessary. Due to the high computing cost of MD, the cooling rate (typically  $10^{14}$ – $10^9$  K/s) is much faster than those achieved in conventional experiments ( $10^2$ – $10^0$  K/s) [Li *et al.*, 2017]. From the viewpoint of PEL [Goldstein, 1969, Wilkinson and Mauro, 2021], the system starts, upon cooling, from a high-energy, ergodic liquid state and gradually evolves to some nonergodic, lower-energy state, before eventually getting trapped in a local minimum corresponding to a glassy state (see Figure 4b) [Debenedetti and Stillinger, 2001]. At the end of the cooling process, it is also common to perform

an additional relaxation run to ensure that the system has reached a plateau in energy, and volume or pressure (in the *NPT* and *NVT* ensembles, respectively).

Fourth, once formed, the glass can be investigated or subjected to additional simulations [Du, 2019, Pedone, 2009]. Typical investigations include various structural analysis (e.g., coordination number) [Bauchy, 2014, 2012], mechanical properties (e.g., strain–stress curve) [Liu *et al.*, 2019b, Yang *et al.*, 2019b], thermodynamics (e.g., potential energy) [Bauchy and Micoulaut, 2015], and vibrational/dynamical properties (e.g., atom diffusivity) [Bauchy *et al.*, 2013, Bauchy and Micoulaut, 2011]. More details can be found in Levchenko *et al.* [2020], Massobrio [2015]. Note that any statistical analysis must be averaged over a trajectory that is long enough to filter out the effect of statistical fluctuations (the magnitude thereof depending on the size of the simulated system). It is also worth noting that, upon quenching, the glass may end up in notably different regions of the energy landscape [Allen and Tildesley, 2017]. As such, it is a good practice to simulate a series of independent melt-quenching simulations for each glass (typically around 3 to 6) and to average results over these simulations.

## 2.4. *Ab initio* molecular dynamics simulations

### 2.4.1. First-principles calculation of interatomic interactions

*Ab initio* MD simulations estimate the interatomic interactions based on first-principles calculation of electron interactions within the framework of density function theory (DFT) [Kohn and Sham, 1965, Marx and Hutter, 2009, Parr, 1980]. Figure 5a illustrates the basic idea of *ab initio* MD, wherein a glass system’s potential energy  $U$  is computed as a function of both the electron wave functions  $\{\Psi_e\}$  (i.e., the electron state) and the nuclei positions  $\{r_n\}$  (i.e., the nuclei state) [Hohenberg and Kohn, 1964, Kohn and Sham, 1965]. The potential energy  $U$  is calculated by summing up three types of interactions in the system [Boero *et al.*, 2015, Marx and Hutter, 2009]:

$$U(\{\Psi_e\}, \{r_n\}) = U_{n-n}(\{r_n\}) + U_{e-n}(\{\Psi_e\}, \{r_n\}) + U_{e-e}(\{\Psi_e\}) \quad (3)$$

where the right-hand terms refer to nucleus–nucleus interactions  $U_{n-n}$ , electron–nucleus interactions  $U_{e-n}$ , and electron–electron interactions  $U_{e-e}$ , respectively.  $U_{e-n}$  can be estimated using the pseudopotential (PP) approach [Hamann *et al.*, 1979, Troullier and Martins, 1991, Vanderbilt, 1990] wherein core electrons (close to the nucleus, where the electron–nucleus interaction varies rapidly in space) are filtered out as they do not engage in the creation of chemical bonding. Rather, interatomic interactions arise from valence electrons (far away from the nucleus) that form chemical bonds [Bachelet *et al.*, 1982]. The PP approach then fits a potential describing the interaction between nucleus and valence electrons, where the fitting uses as reference the all-electron state solution of the ground-state single atom model [Hamann *et al.*, 1979]. Based on the PP approach [Troullier and Martins, 1991],  $U_{n-n}$  is simply the Coulombic interaction between nuclei presenting their net valence charge [Boero *et al.*, 2015].

### 2.4.2. Choice of exchange-correlation (XC) potential

$U_{e-e}$  is a key ingredient in first-principles simulation. It can be further described by three types of energy terms [Boero *et al.*, 2015, Kohn and Sham, 1965]:

$$U_{e-e}(\{\Psi_e\}) = U_{e-e}^{\text{kinetic}} + U_{e-e}^{\text{Coulomb}} + U_{e-e}^{\text{XC}} \quad (4)$$

where the right-hand terms represent the electrons’ kinetic energy  $U^{\text{kinetic}}$ , Coulombic interaction  $U^{\text{Coulomb}}$ , and the exchange-correlation (XC) interaction  $U^{\text{XC}}$ , respectively. Note that, the XC interaction is very challenging to describe accurately [Gunnarsson and Jones, 1985, Johnson *et al.*, 1993, Perdew and Zunger, 1981], as it depends not only on the local electron density but also on its spatial gradient [Langreth and Mehl, 1983, Perdew *et al.*, 1996a]. Assuming that the local electron density is homogeneous, the local density approximation (LDA) method can be used to estimate  $U^{\text{XC}}$  [Fulde, 1995, Kohn and Sham, 1965], which has been proved to offer satisfactory descriptions of XC interactions [Cobb *et al.*, 1996]. However, it should be pointed out that, in many cases (e.g., glasses exhibiting structural heterogeneities [Micoulaut *et al.*, 2013]), assuming a homogeneous local electron density results in an inaccurate estimation of  $U^{\text{XC}}$  [Langreth and Mehl, 1983, Micoulaut *et al.*, 2009]. To address this issue, some generalized gradient approximation (GGA)

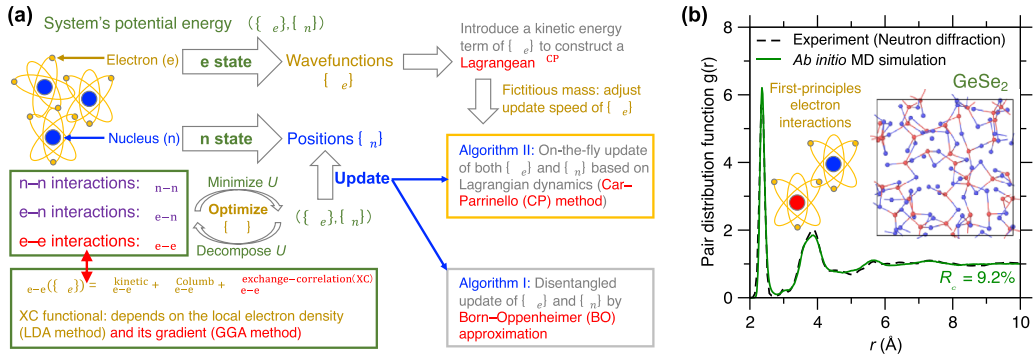


**Figure 5.** (a) Schematic illustrating the basic idea of *ab initio* molecular dynamics (MD) based on first-principles calculation of the system's potential energy  $U$  (see text for details) [Boero et al., 2015]. (b) Comparison between the pair distribution function (PDF)  $g(r)$  computed by neutron diffraction experiment and *ab initio* MD simulation using the Car–Parrinello (CP) method and generalized gradient approximation (GGA) potential for a GeSe<sub>2</sub> glass [Micoulaut et al., 2013]. The inset is a snapshot of the simulated GeSe<sub>2</sub> glass.

methods have been developed to construct more accurate XC functionals with respect to the electron density gradient [Perdew et al., 1996a,b]. More details can be found in Fulde [1995], Marx and Hutter [2009].

### 2.4.3. Numerical algorithms

Based on all these formulations of first-principles interatomic interactions [Boero et al., 2015, Marx and Hutter, 2009], the system's ground-state potential energy  $U(\{\Psi_e\}, \{r_n\})$  can be calculated via optimizing  $\{\Psi_e\}$  so as to minimize  $U$  for the current nuclei positions  $\{r_n\}$  (see Figure 5a) [Hafner, 2008, Pople et al., 1989]. After updating the new nuclei positions  $\{r_n\}$  after a small timestep, the system's potential energy  $U$  is then recomputed through optimizing  $\{\Psi_e\}$  [Boero et al., 2015]. Two algorithms have been developed to optimize  $\{\Psi_e\}$  and update  $\{r_n\}$  [Niklasson et al., 2006], viz., (i) the Born–Oppenheimer (BO) approximation to disentangle the updates of  $\{\Psi_e\}$  and  $\{r_n\}$  [Boero et al., 2015, Niklasson et al., 2006], wherein  $\{\Psi_e\}$  is recomputed at each timestep and offers an accurate estimation of the potential energy  $U$  to update the nuclei positions  $\{r_n\}$ , and (ii) the Car–Parrinello (CP) method to construct a Lagrangian  $L^{\text{CP}}(\{\Psi_e\}, \{r_n\})$  that updates both quantities on-the-fly based on Lagrangian dynamics [Car and Parrinello, 1985], where  $L^{\text{CP}}$  includes a constructed kinetic energy term of

$\{\Psi_e\}$  by assigning to  $\{\Psi_e\}$  a fictitious electronic mass that dictates the update inertia of  $\{\Psi_e\}$  [Boero et al., 2015]. In practice, systems with slow change of nuclei positions tend to require a large fictitious mass to delay the update of  $\{\Psi_e\}$  as well as a large timestep to accelerate the update of  $\{r_n\}$  [Car and Parrinello, 1985]. In other words, when running a CP-MD simulation, one needs to select a proper set of timestep and fictitious mass large enough to (i) reduce the computation cost of the update of  $\{\Psi_e\}$  and  $\{r_n\}$  but also small enough to (ii) numerically conserve the system's energy and linear/angular momentum [Boero et al., 2015]. More details can be found in Boero et al. [2015], Marx and Hutter [2009].

### 2.4.4. Applications and limitations

Since *ab initio* MD simulations are typically able to accurately describe interatomic interactions [Pople et al., 1989], they are the method of choice to simulate complex glasses for which no robust empirical forcefields are available (see below). This is typically the case for glasses exhibiting complex bonds (i.e., with a mixed ionic/covalent/metallic character or varying electronic delocalization) or flexible local structures (e.g., varying coordination numbers) [Massobrio, 2015]. For example, chalcogenide glasses (e.g., Ge–Se glasses) typically exhibit complex structural features that cannot be accurately

reproduced by classical MD [Mauro and Varshneya, 2006], including under- and over-coordinated atoms, edge-sharing structures, and homopolar bonds (see insert of Figure 5b) [Petri *et al.*, 2000]. Figure 5b shows a melt-quenched GeSe<sub>2</sub> glass prepared by *ab initio* MD simulation, wherein its computed PDF  $g(r)$  is compared with neutron diffraction data [Micoulaut *et al.*, 2013]. Relying on CP-MD method and GGA-XC potential [Car and Parrinello, 1985, Perdew *et al.*, 1996a], the simulation offers a glass structure that is in excellent agreement with experimental data [Micoulaut *et al.*, 2009].

However, despite their unparalleled predictive power [Pople *et al.*, 1989], *ab initio* simulations still come with a series of limitations. First, although they rely on a fundamental description of electronic interactions, they still rely on a number of assumptions (e.g., choice of the pseudopotential and exchange-correlation function). Second, *ab initio* MD simulations come with a computational cost that is orders of magnitude larger than that of classical MD [Marx and Hutter, 2009]. This limits the timescale that is accessible to *ab initio* MD simulations (typically to 100s of ps) [Boero *et al.*, 2015]. This restricts their use to high cooling rates, which, in turn, tends to yield glasses that are more disordered (higher fictive temperature) than their experimental counterparts [Li *et al.*, 2017]. Finally, the computational cost of *ab initio* MD simulations typically scales with the cube of the number of electronic degrees of freedom [Hafner, 2008]. As a result, *ab initio* MD simulations are usually limited to very small systems (up to a few hundred atoms) [Massobrio, 2015]. This prevents their use in capturing small compositional effects (since replacing one atom by another largely affects the overall composition in a small system) or extended structural features (e.g., large rings or compositional heterogeneity) [Du and Corrales, 2006, Nakano *et al.*, 1994].

Thanks to their accuracy, *ab initio* MD simulations have been applied to predict the structure and dynamics of various types of glasses or amorphous solids, including amorphous silicon [Car and Parrinello, 1988], chalcogenide [Micoulaut *et al.*, 2013], Ge-Sb-Te phase-change materials [Caravati *et al.*, 2009], MOFs [Darby *et al.*, 2020, Sillar *et al.*, 2009], silicates [Baral *et al.*, 2017, Tilocca and de Leeuw, 2006], borates [Scherer *et al.*, 2019], etc. Notably, by accurately describing the interatomic interactions, *ab ini-*

*tio* MD offers a powerful tool to simulate complex glasses that cannot be properly described by empirical forcefields.

## 2.5. Classical molecular dynamics simulations

### 2.5.1. Empirical forcefields

In contrast to the explicit description of electronic effects offered by *ab initio* MD [Marx and Hutter, 2009], classical MD relies on empirical forcefields to describe interatomic interactions—via physics/intuition-based, computationally efficient functionals [Massobrio, 2015]. For example, Figure 6a shows the PDF  $g(r)$  of a melt-quenched (Na<sub>2</sub>O)<sub>30</sub>(SiO<sub>2</sub>)<sub>70</sub> glass prepared by classical MD simulation using an empirical forcefield [Cormack *et al.*, 2002, Du and Cormack, 2004]. The neutron diffraction data is added as a reference for comparison [Wright *et al.*, 1991]. Notably, this empirical forcefield offers an atomistic structure that is in good agreement with experimental data. Note that the simulated and experimental glasses are prepared with different cooling rate [Li *et al.*, 2017]. The good agreement between simulated and experimental PDFs (see Figure 6a) suggests that, although the empirical forcefield is a simplification of the real interatomic interactions [Huang and Kieffer, 2015, van Beest *et al.*, 1990], it can accurately describe them while relying on a significantly reduced computational cost as compared to first-principles calculations [Bauchy *et al.*, 2013, Carré *et al.*, 2008]. Thanks to its much faster execution time as compared to *ab initio* MD simulation, classical MD simulation can extend to much longer timescales (up to a few nanoseconds) and larger length scales (up to millions of atoms) [Lane, 2015, Plimpton, 1995a].

### 2.5.2. Forcefield functionals

The optimal functional form of the empirical interatomic potential depends on the type of glass that is simulated (e.g., ionic, covalent, metallic glass, etc.) and no “universal” empirical potential is available to date [Du, 2015, Huang and Kieffer, 2015].

In practice, ionocovalent glasses (e.g., silicate glasses, which feature ionocovalent bonds [Huang and Kieffer, 2015]) can be well described by a combination of: (i) long-range coulombic interactions and (ii) a Buckingham-format functional description

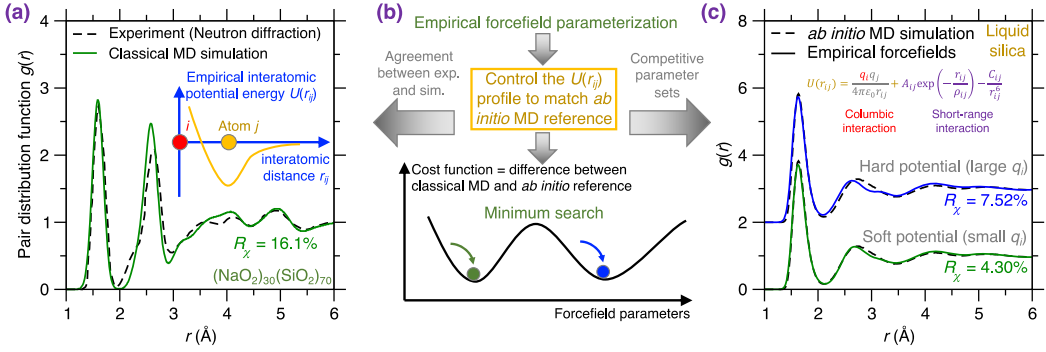


**Figure 6.** (a) Pair distribution function (PDF)  $g(r)$  of a melt-quenched  $(\text{NaO}_2)_{30}(\text{SiO}_2)_{70}$  glass prepared by a classical MD simulation using an empirical forcefield (here, a Buckingham potential [Cormack et al., 2002], see (5)) and a cooling rate of 0.001 K/ps [Zhou et al., 2020]. The neutron diffraction data is added as a comparison [Wright et al., 1991]. The inset illustrates the shape of this empirical forcefield, i.e., the interatomic potential energy  $U(r_{ij})$  as a function of interatomic distance  $r_{ij}$  [van Beest et al., 1990]. (b) Schematic illustrating the parameterization of an empirical forcefield by searching for the minimum position (i.e., the optimal forcefield) in a cost function landscape as a function of forcefield parameters [Carré et al., 2016]. The cost function is defined herein as the difference between classical MD result and its *ab initio* reference [Liu et al., 2019e]. The optimal forcefield is parameterized so as to match *ab initio* MD simulation and also offers a good agreement with experiment (see panel (a)) [Carré et al., 2008]. Note that several competitive minima (yielding competitive optimal forcefields) can coexist in the cost function landscape (see panel (c)) [Liu et al., 2020a]. (c) Comparison between the PDFs computed by *ab initio* MD simulation and classical MD simulation using two distinct Buckingham forcefields (with different parameterizations) for a silica liquid. The two potentials are referred to as “soft” (exhibiting weak columbic interactions) and “hard” (exhibiting more intense columbic interactions) [Liu et al., 2020a].

of short-range interactions to compute the potential energy  $U(r_{ij})$  between atom  $i$  and atom  $j$  at a distance  $r_{ij}$  (see inset of Figure 6a) [Carré et al., 2008, Du and Corrales, 2006, van Beest et al., 1990]:

$$U(r_{ij}) = \frac{q_i q_j}{4\pi\epsilon_0 r_{ij}} + A_{ij} \exp\left(-\frac{r_{ij}}{\rho_{ij}}\right) - \frac{C_{ij}}{r_{ij}^6} \quad (5)$$

where  $q_i$  is the partial charge of atom  $i$ ,  $\epsilon_0$  is the dielectric constant, and  $A_{ij}$ ,  $\rho_{ij}$ , and  $C_{ij}$  are parameters describing short-range interactions [Du and Corrales, 2006]. These parameters are adjusted for each pair of elements (e.g., Si–O) so as to achieve a good agreement with experimental or *ab initio* references (see below) [Sundaraman et al., 2018, van Beest et al., 1990]. In particular, the well-established Teter potential [Cormack et al., 2002] has been demonstrated to offer an accurate description of various structural, thermodynamical, and dynamical properties of silicate glasses [Bauchy, 2012, Bauchy et al., 2013, Du and Cormack, 2004, Du and Corrales, 2006].

Note that, in the case of interactions that rapidly converge to zero upon increasing distance (e.g., Van der Waals interactions, which is proportional to  $1/r^6$ ), the energy error associated with the fact of using a finite cutoff converges to zero as the cutoff increases. However, this is not the case for Coulombic interactions, which exhibit a slow decrease upon increasing distance  $r$  (i.e., proportional to  $1/r$ ). In such a case, the energy contribution that is neglected when using a cutoff (arising from long-distance interactions between atoms) does not converge to zero upon increasing cutoff. As such, long-range Coulombic interactions (including across PBC) must be explicitly considered to ensure the accuracy of the simulation. In practice, computing Coulombic interactions is often the most computationally expensive step when simulating ionocovalent glasses. In that regard, various summation methods have been developed to speed up the computation of electrostatic interactions, such as the Ewald method [Ewald, 1921],

particle–particle–particle–mesh (PPPM) method [Hockney and Eastwood, 1988], and damped-shifted-force (DSF) method [Fennell and Gezelter, 2006]. In detail, both the Ewald and PPPM methods are based on the idea that the summation of long-range interactions can be efficiently calculated in the reciprocal space using a Fourier transform [Allen and Tildesley, 2017]. Unlike the Ewald or PPPM methods, the DSF method is conducted in real space and is based on the rapidly converging summation of a short-range potential—whose cutoff is large enough—to approach the effective long-range Coulombic interactions [Fennell and Gezelter, 2006]. In practice, both the Ewald and PPPM summation methods offer accurate calculations of the Coulombic interactions. In many cases, electrostatic interactions can also be reasonably well approximated by the DSF method [Carré *et al.*, 2007, Fennell and Gezelter, 2006], which, in turn, is significantly more computationally efficient than Ewald and PPPM since it does not involve any Fourier transform [Fennell and Gezelter, 2006].

It is worth pointing out that, as the accuracy of classical MD simulations significantly relies on the analytical formulation of the empirical forcefield, it is necessary, when developing empirical forcefield functionals, to account for all essential components of the interaction (e.g., Coulombic component of ionocovalent interaction) that affect the targeted glass properties. Indeed, although select properties are not very sensitive to the details of a forcefield (e.g., density or PDF), other properties can be strongly affected by small variations in the parameters or analytical formulation of the empirical potential. In such cases, it may be necessary to develop advanced forcefields that are able to capture some complex chemical or physical behaviors, including bond formation/breaking, charge transfers, polarization effects, short-range repulsion, etc. [Jahn *et al.*, 2006, Jahn and Madden, 2007, Serva *et al.*, 2020]. In that regard, some advanced forcefields such as the aspherical ion model (AIM)—which is more complex than the Buckingham potential [Liu *et al.*, 2020a]—have been developed to account for these essential, complex interaction behaviors in studying the dynamics of complex oxides [Jahn *et al.*, 2006, Jahn and Madden, 2007, Serva *et al.*, 2020]. Note that, although such potentials are more computationally expensive, they generally show an improved level of agreement with experiments and a high transferability upon composi-

tion, temperature, and pressure changes [Jahn *et al.*, 2006, Jahn and Madden, 2007, Serva *et al.*, 2020].

In contrast to ionocovalent glasses, covalent glasses (e.g., amorphous silicon [Stillinger and Weber, 1985] or chalcogenide glasses [Micoulaut *et al.*, 2013]) cannot be described by 2-body interatomic potentials due to the directional nature of the covalent bonds they form [Phillips, 1981, 1979]. As such, describing covalent glasses requires the use of 3-body potential interactions—e.g., Stillinger–Weber (SW) potential [Ding and Andersen, 1986, Stillinger and Weber, 1985]—to constraint the values of the interatomic angular interactions between a central atom  $i$  and its two neighbor atoms  $j$  and  $k$  [Du, 2015, Mauro and Varshneya, 2006]:

$$U(r_{ij}, r_{ik}, \theta_{ijk}) = \sum_i \sum_{j>i} \phi_2(r_{ij}) + \sum_i \sum_{j \neq i} \sum_{k>j} \phi_3(r_{ij}, r_{ik}, \theta_{ijk}) \quad (6)$$

where  $\phi_2$  and  $\phi_3$  represent, respectively, the radial 2-body interaction and angular 3-body interaction term, as a function of the interatomic distance  $r_{ij}$ ,  $r_{ik}$ , and the bond angle  $\theta_{ijk}$  between the vectors  $r_{ij}$  and  $r_{ik}$ . More details can be found in Du [2019], Mauro and Varshneya [2006], Stillinger and Weber [1985].

Finally, the simulation of metallic glasses typically requires the description of many-body effects [Pelletier and Qiao, 2019, Sheng *et al.*, 2006], which can be well described by the Embedded Atom Method (EAM) potential [Daw *et al.*, 1993]. In the EAM approach, the potential energy  $U_i$  of a central atom  $i$  is formulated as [Daw and Baskes, 1984, 1983]:

$$U_i = f_\alpha \left( \sum_{j \neq i} \rho \beta(r_{ij}) \right) + \frac{1}{2} \sum_{j \neq i} \phi_{\alpha\beta}(r_{ij}) \quad (7)$$

where  $F$  is the energy gained by embedding the cation  $i$  in the “ocean” of delocalized electrons described by the local atomic electron density  $\rho$ ,  $\phi$  is a pair potential interaction describing the cation–cation interactions,  $\alpha$ ,  $\beta$  represent element type of atom  $i$  and  $j$ , respectively, and  $j$  denotes the neighbors of atom  $i$  within a radius cutoff  $r_c$ . More details can be found in Daw *et al.* [1993], Daw and Baskes [1983].

Note that, to reduce the computational cost associated with the calculation of the empirical forcefields, a cutoff  $r_c$  is typically adopted—wherein the interaction energy between a pair of atoms is assumed to be zero if their distance exceeds the cutoff

[Chialvo and Debenedetti, 1990, Du, 2015]. In addition, a neighbor list algorithm is typically adopted to reduce the number of times the distance between a pair of atoms is calculated [Allen and Tildesley, 2017, Leach, 2001].

### 2.5.3. Forcefield parameterization

In addition to the choice of its functional form [Du, 2015], the accuracy of an empirical forcefield strongly depends on its parameterization [Sundararaman *et al.*, 2020, 2018, Wang *et al.*, 2018]. Figure 6b illustrates the general idea behind the parameterization of an empirical potential. Such parameterization can be formulated as an optimization problem, wherein the forcefield parameters are optimized so as to minimize a given cost function. This problem can be illustrated in terms of a cost function landscape, which represents the topographical evolution of the cost function as a function of the forcefield parameters. The cost function captures the level of mismatch between a simulated metric and a given reference value. The simulated metric can be the interatomic energy/force, some structural features (e.g., PDF), or some other macroscopic properties (e.g., density, stiffness, etc.).

For each type of metric, reference values can be offered by experimental data or *ab initio* simulations. On the one hand, defining the cost function in terms of the level of mismatch between computed and experimental data tends to yield a good agreement between simulated and experimental glass properties—since the parameterization scheme specifically aims to minimize this difference. However, on the other hand, it is not always meaningful to compare a simulated glass with its experimental counterpart. Indeed, glasses simulated by MD are prepared with a cooling rate that is significantly higher than those experienced in traditional experiments and, therefore, should be different (typically more disordered) than their experimental counterparts [Carré *et al.*, 2016, Li *et al.*, 2017, Vollmayr *et al.*, 1996b]. Hence, parameterizing an empirical forcefield so as to “force” a simulated glass to exhibit properties that match experimental data may yield an unrealistic forcefield. That is, forcing simulated and experimental glasses to feature similar properties can typically only be achieved by “mutual compensations of errors”, that is, wherein the forcefield is deformed so as to compensate the fact that the simulated glass is prepared

with an extremely high cooling rate. As such, although such parameterization may offer an apparent agreement between simulations and experiments for the properties that are included in the cost function, the resulting forcefield, due to its nonphysical nature, may dramatically fail at predicting properties that are not included in its cost function. In contrast, parameterizing a forcefield so as to match with *ab initio* data is expected to yield a more realistic description of the true interatomic potential. However, glasses prepared with such a realistic forcefield should be compared to hyperquenched glasses (i.e., prepared under high cooling rate) and, hence, may not exhibit a good agreement with experimental data prepared under slower cooling rates.

In terms of the metric to be considered in the cost function, it has recently been suggested that, in the case of glasses or liquids, using a structural property as reference (e.g., PDF) tends to offer better results than directly forcing the parameterized forcefield to match reference force values (as computed by *ab initio* simulations) [Carré *et al.*, 2016, 2008]. In the example shown in Figure 6c, the cost function  $R_\chi$  is defined as the magnitude of the difference between the PDF  $g(r)$  computed by classical MD and *ab initio* MD for a liquid silica system [Liu *et al.*, 2019e]. Note that parameterizing this forcefield based on liquid (rather than glassy) configurations effectively removes any spurious effects arising from the thermal history of the system.

Various optimization methods are available to “navigate” the cost function landscape, that is, to identify the optimal forcefield parameters that minimize the cost function [Carré *et al.*, 2016], including MC search [Iype *et al.*, 2013], Bayesian optimization [Liu *et al.*, 2019c,e], particle swarm optimization [Christensen *et al.*, 2021], or gradient descent search [Shewchuk, 1994]. Note that this optimization problem is typically ill-defined since several degenerate sets of forcefield parameters can often minimize the cost function, that is, several competitive minimum positions can be found in the cost function landscape [Liu *et al.*, 2020a, 2019c]. Figure 6c illustrates two competitive forcefields based on the same Buckingham-format functional [van Beest *et al.*, 1990] (see (5)). These forcefields can be described as “soft” (featuring weak coulombic interactions) and “hard” (featuring more intense coulombic interactions) and both offer a competitive mini-



mum value of the cost function  $R_\chi$  for silica liquids [Liu *et al.*, 2020a]. Nevertheless, despite the apparent harmony, the atomistic structures offered by the soft and hard potential exhibit pronounced differences for structural features that are not included in the cost function (e.g., bond angular distribution or ring size distribution) [Liu *et al.*, 2020a]. This exemplifies the need to *a posteriori* validate forcefields that validate the accuracy of forcefields after their parameterization [Liu *et al.*, 2019c].

Finally, it is worth pointing out that both the choice of forcefield functionals and forcefield parameterization can affect the forcefield's transferability as a function of, for instance, glass composition, pressure, or temperature [Hernandez *et al.*, 2019, Jahn and Madden, 2007]. Indeed, forcefields are often developed for a specific glass composition and range temperature/pressure (e.g., liquid silica). In general, there is no guarantee that such forcefields can offer realistic predictions far from the conditions used during their training [Sundararaman *et al.*, 2020, 2018]. For instance, certain chemical behaviors—e.g., charge transfers—may not be similar under various conditions of temperature or pressure and, hence, may require some adjustments in the parameterization of empirical forces to be properly accounted for [Liu *et al.*, 2020a]. The transferability of forcefields is also likely to be poor when the forcefield is used under conditions wherein the atoms exhibit some local environments (e.g., varying coordination numbers) that are different from those observed during the training of the forcefield. This limitation is especially pronounced for borate glasses (wherein the average coordination number of boron depends on temperature) and pressurized glasses (wherein coordination numbers tend to increase under pressure) [Salmon and Zeidler, 2015]. In order to overcome these limitations and develop transferable forcefields, one first needs to propose a forcefield functional that is complex enough to capture the nature of interatomic interactions in all the conditions of interest (e.g., Buckingham-format potential for ionocovalent bond interactions in silicate glasses), but generic enough to avoid any unrealistic extrapolations due to “overfitting” [Du, 2015, Huang and Kieffer, 2015]. Then, the transferability of a forcefield greatly depends on its forcefield parameterization scheme, where the cost function should be designed so as to consider the structure and properties of glasses under different

conditions [Liu *et al.*, 2019c, Sundararaman *et al.*, 2018]. Note that there always exists a balance between (i) the ability of a forcefield to accurately predict the unique, detailed properties of a specific system and (ii) the capability of a forcefield to offer a robust transferability for a wide range of compositions and conditions [Liu *et al.*, 2019c]. To address the issue of transferability, several recent works have focussed on developing generic forcefields that can be applied to a large compositional envelope at the expense of potentially being unable to capture the fine structural details of a specific composition [Hernandez *et al.*, 2019, Jahn and Madden, 2007], including the well-established Teter potential for modified silicate glasses [Du and Corrales, 2006], the Wang–Bauchy potential for borosilicate glasses [Wang *et al.*, 2018], etc.

Thanks to their high computational efficiency as compared to *ab initio* simulations [Carré *et al.*, 2008, Huang and Kieffer, 2015], classical MD simulations relying on empirical forcefields have been extensively used to model glasses [Cormier *et al.*, 2003, Mead and Mountjoy, 2006, Tanguy *et al.*, 1998]. Simulated systems include glassy silica [Carré *et al.*, 2008, Liu *et al.*, 2020a, van Beest *et al.*, 1990], modified (e.g., alkali) silicate glasses [Cormack and Du, 2001], aluminosilicate glasses [Bouhadja *et al.*, 2013], borates [Kieu *et al.*, 2011, Sundararaman *et al.*, 2020, Wang *et al.*, 2018], etc. It should be pointed out that, as the number of elements in the glass increases, it becomes extremely challenging to properly describe all the distinct interactions between pair of elements (since the number of parameters that need to be adjusted scales with the square of the number of elements) [Du, 2015].

## 2.6. Reactive molecular dynamics simulations

### 2.6.1. Gap between *ab initio* and classical MD simulations

In contrast to classical MD, *ab initio* MD can accurately describe a chemical reaction process but is limited to small system size (up to hundreds of atoms) [Boero *et al.*, 2015], while, in turn, classical MD can extend to large systems (up to millions of atoms) but lack an accurate description of chemical reaction processes [Plimpton, 1995a, Senftle *et al.*, 2016]. Although classical MD simulations

exhibit high computation efficiency [Marx and Hutter, 2009, Massobrio, 2015], they rely on simplified empirical forcefields, which may accurately predict certain properties (e.g., PDF  $g(r)$ ) of glasses but may not offer robust predictions for more complex properties that are more sensitive to the details of the forcefields [Ganster *et al.*, 2007, Ispas *et al.*, 2002]. In addition, classical MD simulations relying on static forcefields and fixed charges are often unable to robustly account for charge transfer mechanisms and defective coordinated states, which prevents such simulations from properly describing the breaking and formation of bonds during chemical reactions [Buehler *et al.*, 2006, Deng *et al.*, 2021, Du *et al.*, 2019a, Yu *et al.*, 2018]. To address this limitation, reactive MD simulations—i.e., MD relying on reactive forcefields (e.g., ReaxFF) [van Duin *et al.*, 2003, 2001]—have been proposed as an intermediate option, in between classical and *ab initio* MD. The promise of reactive MD is to offer an accuracy that approaches that of *ab initio* MD while involving a computational burden that is more comparable to that of classical MD. This makes it possible for reactive MD to simulate fairly large systems (up to tens of thousands of atoms) over extended time scales (up to a few nanoseconds) with an enhanced accuracy as compared to classical MD (see Figure 7a) [Senftle *et al.*, 2016]. However, reactive forcefields typically rely on hundreds-to-thousands of parameters and, hence, are extremely challenging to parameterize. This has thus far limited their applications to a small number of glass families [Senftle *et al.*, 2016].

### 2.6.2. ReaxFF forcefield

The ReaxFF forcefield is one of the most popular implementations of reactive MD [Leven *et al.*, 2021]. As detailed in the following, the key advantages of ReaxFF are that it (i) explicitly describes the dynamical formations and breaking of bonds, (ii) accounts for charge transfers between atoms, and (iii) dynamically adjusts the interatomic interactions as a function of the local environment of each atom [van Duin *et al.*, 2003, 2001]. This makes it possible to describe phase transitions, defect formations, or chemical reactions between atoms (e.g., to simulate the reactivity of a glass surface with water) [Buehler *et al.*, 2006, Du *et al.*, 2018].

In detail, the ReaxFF forcefield calculates the sys-

tem's potential energy  $U_{\text{sys}}$  by summing up the following energy terms [van Duin *et al.*, 2003]:

$$U_{\text{sys}} = U_{\text{bond}} + U_{\text{vdWaals}} + U_{\text{Coulomb}} + U_{\text{under}} + U_{\text{over}} + U_{\text{lp}} + U_{\text{val}} + U_{\text{tors}} + U_{\text{conj}} + U_{\text{pen}} \quad (8)$$

where the right-hand terms refer, respectively, to the short-range bond energy, Van der Waals energy, Coulomb potential energy, under-coordination energy, over-coordination energy, long-range electron pairs energy, valence angle energy, torsion energy, conjugation energy, and penalty energy. A detailed description of these terms can be found in Senftle *et al.* [2016], van Duin *et al.* [2003, 2001]. Importantly, ReaxFF is a bond-order-based forcefield, that is, the energy terms are generally formulated as a function of the local bond order of each atom, which is dynamically determined by its local environment [van Duin *et al.*, 2003]. This bond-order formulation enables reactive MD to capture the dynamical process of bond formations and dissociations. Moreover, in contrast to classical MD simulations relying on fixed charges [Liu *et al.*, 2019e, van Beest *et al.*, 1990], the charges of the atoms are dynamically assigned based on a charge equilibration (QEq) method [Rappe and Goddard, 1991], which captures the occurrence of charge transfers during bond breakages and reformations. All these features—i.e., dynamical bond formations and charge transfers—render ReaxFF ideal to simulate chemical reactions [Senftle *et al.*, 2016].

### 2.6.3. Glass reactivity

Reactive MD simulations offer an ideal tool to investigate the chemical reactivity of glasses [Senftle *et al.*, 2016]. For instance, Figure 7b illustrates the sol-gel formation process of glassy silica (in terms of the condensation of  $\text{Si}(\text{OH})_4$  precursors) from the viewpoint of an energy state transition in PEL [Du *et al.*, 2018, Steinfeld *et al.*, 1999]. Classical MD relying on empirical forcefield (e.g., Buckingham potential [van Beest *et al.*, 1990]) generally offers an accurate description of near-equilibrium properties (i.e., around local minimum energy states) but typically fails at properly describing far-from-equilibrium behaviors like those experienced in transition states [Liu *et al.*, 2019e]. In particular, classical MD typically does not offer realistic energy barrier predictions [Du *et al.*, 2018]. In contrast, reactive MD (e.g., based on ReaxFF) can offer more accurate description of transition energy barriers, which makes it possible to

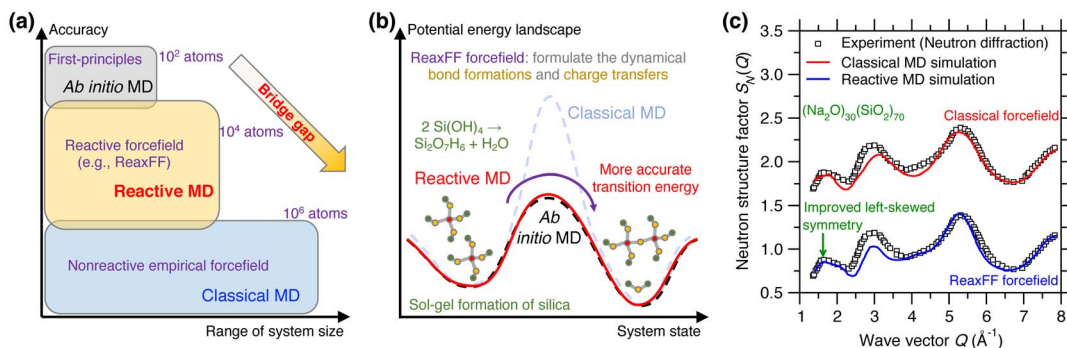


**Figure 7.** (a) Illustration of reactive molecular dynamics (MD) simulations relying on reactive forcefield (e.g., ReaxFF) to bridge the gap between *ab initio* and classical MD, both in terms of range of system size and accuracy [Senftle *et al.*, 2016]. (b) Illustration of the sol-gel formation process of glassy silica in terms of the potential energy landscape (PEL) predicted by *ab initio* MD, reactive MD, and classical MD [Du *et al.*, 2018, Steinfeld *et al.*, 1999]. Using the *ab initio* PEL as a reference, reactive MD shows a more accurate transition energy than classical MD [Du *et al.*, 2018], on account of the fact that the ReaxFF forcefield explicitly models dynamical bond formations and charge transfers during the chemical reaction [van Duin *et al.*, 2003]. (c) Comparison between the neutron structure factor  $S_N(Q)$  computed by classical MD and reactive MD for a sodium silicate glass ((Na<sub>2</sub>O)<sub>30</sub>(SiO<sub>2</sub>)<sub>70</sub>) [Yu *et al.*, 2017a]. The same experimental  $S_N(Q)$  is added as a reference [Grimley *et al.*, 1990].

simulate sol-to-gel transitions [Du *et al.*, 2019b, 2018, Zhao *et al.*, 2021, 2020]. Reactive potentials also make it possible to model the reactivity of glass with aqueous solutions [Deng *et al.*, 2019, Du *et al.*, 2019a, Fogarty *et al.*, 2010, Mahadevan and Du, 2020, Yu *et al.*, 2018]. The description of bond formation/breaking also make reactive MD simulations an ideal tool to study fracture processes [Bauchy *et al.*, 2016, 2015, To *et al.*, 2020] or vapor deposition processes [Wang *et al.*, 2020].

#### 2.6.4. Glass structure

The fact that ReaxFF can dynamically adjust interatomic interactions as a function of the local environment of each atom is also a key advantage in glass simulations—since glasses can exhibit a large variety of local structures (e.g., varying coordination states). As such, when properly parameterized, reactive forcefields have the potential to offer an improved description of the atomic structure of glasses as compared to classical MD [Yu *et al.*, 2017a, 2016]. Figure 7c shows a comparison between the neutron structure factor  $S_N(Q)$  computed by classical and reactive MD simulation for a (Na<sub>2</sub>O)<sub>30</sub>(SiO<sub>2</sub>)<sub>70</sub> glass [Yu *et al.*, 2017a]. Taking the experimental  $S_N(Q)$  as a reference [Grimley *et al.*, 1990], reactive MD relying

on the ReaxFF forcefield offers an improved description of the medium-range structure (e.g., improved left-skewed symmetry of  $S_N(Q)$  at low- $Q$  region [Yu *et al.*, 2017a]) as compared to that offered by classical MD relying on a Buckingham forcefield [Du and Cormack, 2004]. The ability of ReaxFF to properly handle coordination defects also makes it an ideal tool to study irradiation-induced vitrification [Krishnan *et al.*, 2017a,c, Wang *et al.*, 2017].

Although its application to glassy systems has thus far remained fairly limited, the ReaxFF forcefield has been used to model several noncrystalline systems, including amorphous silicon [Buehler *et al.*, 2006], glassy silica [Yu *et al.*, 2016], sodium silicate glasses [Deng *et al.*, 2020], modified aluminosilicate glasses [Dongol *et al.*, 2018, Liu *et al.*, 2020c, Mahadevan and Du, 2021], organosilicate glasses [Rimsza *et al.*, 2016], and zeolitic imidazolate frameworks (ZIFs) [Yang *et al.*, 2018], etc. Despite the unique advantages offered by ReaxFF, its applications are presently limited by the range of elements that have been parameterized [Leven *et al.*, 2021, Senftle *et al.*, 2016].

### 3. Grand challenges in atomistic simulations of glasses

#### 3.1. Parameterization of empirical forcefields

##### 3.1.1. High dimensionality

Empirical forcefields involve many parameters that need to be optimized [Liu *et al.*, 2019c]. For example, ReaxFF forcefields generally comprise hundreds (or thousands) of parameters [van Duin *et al.*, 2003]. Although classical forcefields are usually simpler, they still involve dozens of parameters—a number that increases upon increasing number of elements [Huang and Kieffer, 2015]. Such high dimensionality makes it challenging to identify optimal values for the parameters, that is, to reliably find the minimum position in the cost function landscape [Carré *et al.*, 2016, Shewchuk, 1994].

##### 3.1.2. Roughness of cost function landscape

Figure 8a illustrates a cost function landscape as a function of arbitrary forcefield parameters, where the cost function  $R_\chi$  is defined herein as the magnitude of difference between the PDF  $g(r)$  computed by classical MD and its *ab initio* reference [Liu *et al.*, 2019e]. Since the landscape is rough and features many local minima, traditional gradient-descent-based optimization algorithms are usually largely inefficient since they tend to get stuck in local minima—so that the outcome of the optimization strongly depends on the initial starting point [Shewchuk, 1994].

As an illustrative example, Figure 8b shows the cost function landscape of a Buckingham forcefield for glassy silica as a function of two forcefield parameters (i.e., the silicon partial charge  $q_{\text{Si}}$  and the short-range Si–O interaction intensity  $A_{\text{SiO}}$ ) [Liu *et al.*, 2019e]. Even for this simple system, the cost function landscape is rough and exhibits several local minima. As a result, optimizations relying on conjugated gradient descent [Shewchuk, 1994] tend to get easily stuck at the positions nearby the start point (see Figure 8b) [Liu *et al.*, 2019e]. Indeed, although the cost function looks fairly smooth at a high level, a closer inspection reveals that the cost function locally features a very rough landscape showing a large number of local minima (see bottom panel in Figure 8b) [Liu *et al.*, 2019e]. Overall, as a consequence

of the rough nature of typical cost function landscapes, forcefield parameterization schemes are often strongly biased, heavily relying on intuition, or requiring a large number of independent optimization (with different starting points) [Liu *et al.*, 2019e,c].

#### 3.2. Effect of the cooling rate

##### 3.2.1. Importance of thermal history

Due to the short timescale that is accessible to MD simulations (up to a few nanoseconds trajectories) [Plimpton, 1995a], glass simulations relying on the melt-quenching approach are limited to ultra-fast cooling rates ( $10^{14}$ – $10^9$  K/s), which far exceed the cooling rates achieved in conventional experiments ( $10^2$ – $10^0$  K/s) [Li *et al.*, 2017]. This is important since, glasses being out-of-equilibrium phases, their structure and properties depend on their thermal history. Specifically, glasses tend to reach deeper positions in their PEL upon decreasing cooling rates (i.e., they become more stable, see Figure 9a) [Debenedetti and Stillinger, 2001].

Figure 9b illustrates the evolution of the potential energy  $U$  of a glass with respect to the decreasing temperature during melt-quenching with varying cooling rates: (i) MD simulation with a large cooling rate (typically 10 K/ps), (ii) MD simulation with a slow cooling rate (typically  $10^{-3}$  K/ps), and (iii) experimental melt-quench (typically  $10^{-12}$  K/ps) [Debenedetti and Stillinger, 2001]. At high temperature, the three systems are at the equilibrium liquid state and, hence, exhibit the same potential energy  $U$  [Debenedetti and Stillinger, 2001]. As temperature decreases,  $U$  decreases (the slope depending on the heat capacity of the liquid) and all three systems enter into the metastable supercooled liquid state following the same linear master curve [Debenedetti and Stillinger, 2001]. From this point, the transition from the metastable supercooled liquid state to the out-of-equilibrium glassy state (i.e., at the glass fictive temperature  $T_f$ ) occurs when the relaxation time of the system exceeds the observation time. Although, at fixed temperature, all the three systems exhibit the same relaxation time, the observation time is significantly lower in MD simulations, especially upon large cooling rate. As such, glasses simulated by MD using a large cooling rate enter the glassy state at higher temperature and remain stuck in high-energy states in the PEL (see Figures 9a and b) [Debenedetti

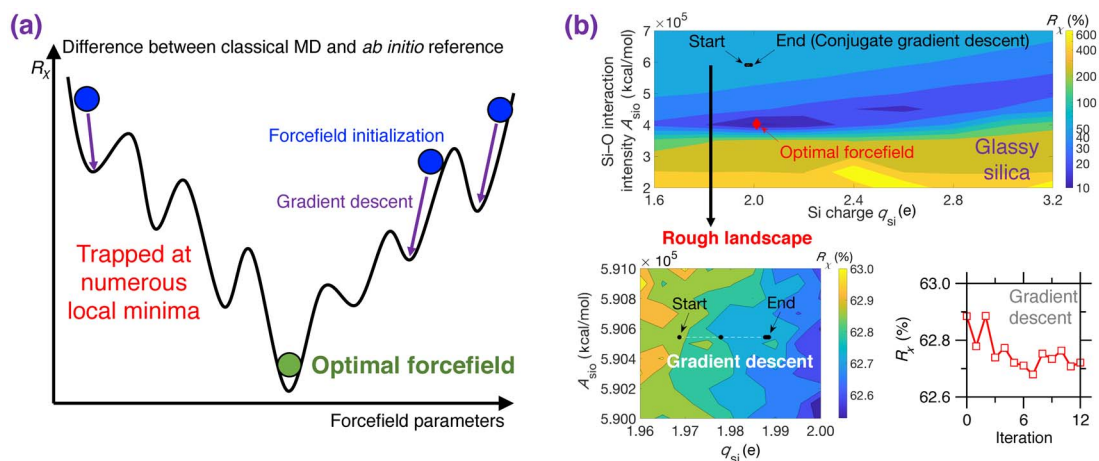


**Figure 8.** (a) Illustration of the rough nature of typical cost function  $R_\chi$  landscapes for empirical forcefield parameterization.  $R_\chi$  is defined herein as the difference between a classical MD result (e.g., PDF) and its *ab initio* reference [Liu et al., 2019e]. The outcome of a typical gradient descent optimization can easily get stuck at numerous local minima and, hence, strongly depends on the initial starting point [Liu et al., 2019e, Shewchuk, 1994]. (b) Contour plot of the cost function  $R_\chi$  associated with a Buckingham potential for glassy silica as a function of two forcefield parameters  $q_{\text{si}}$  and  $A_{\text{sio}}$  (see (5)) [Liu et al., 2019e]. For illustration purposes, the other parameters are fixed based on the well-established van Beest–Kramer–van Santen (BKS) potential [van Beest et al., 1990]. By using conjugated gradient descent [Shewchuk, 1994], the optimization easily gets trapped in a local minimum due to the rough nature of the cost function landscape (see bottom panels), so that the optimization fails to identify optimal forcefield parameters that minimize the cost function [Liu et al., 2019e].

and Stillinger, 2001]. As a result, glasses simulated by MD strongly depend on the choice of the cooling rate and tend to be more stable (i.e., lower final energy  $U_0$ , more ordered) upon decreasing cooling rates.

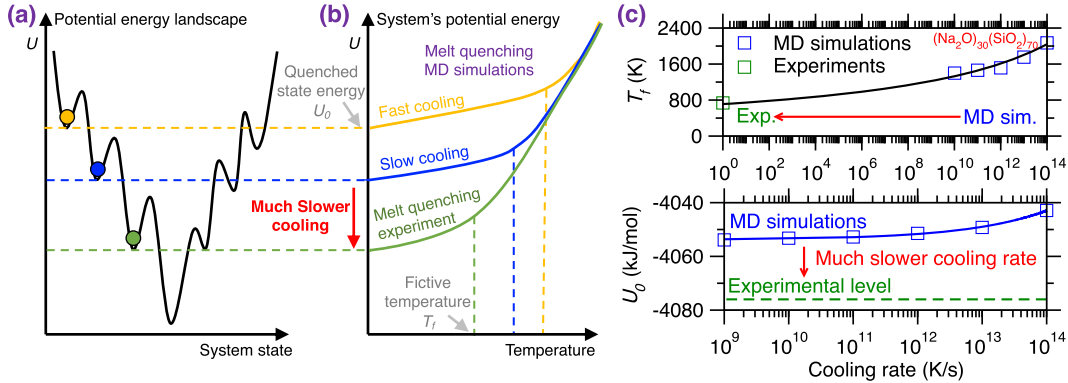
### 3.2.2. Gap between simulated versus experimental glasses

Figure 9c shows the evolution of the glass fictive temperature  $T_f$  and final potential energy  $U_0$  as a function of the cooling rate for both melt-quenching experiments and MD simulations—using the case of a  $(\text{Na}_2\text{O})_{30}(\text{SiO}_2)_{70}$  glass as an archetypical example [Li et al., 2017, Zhou et al., 2020]. As expected, slower cooling rates result in lower  $T_f$  and  $U_0$ . However, due to the huge gap between the cooling rates that are accessible to experiments and simulations [Li et al., 2017], experimental values of  $T_f$  and  $U_0$  tend to be much lower than their simulation counterparts [Li et al., 2017, Zhou et al., 2020]. This difference in the order of the magnitude of the cooling rate is a critical

limitation of MD simulations since it results in a systematic difference between experimental and simulated glasses [Li et al., 2017, Vollmayr et al., 1996b]. Note that different types of glasses may exhibit various dependence on the cooling rate, so that certain glasses are more sensitive to variations in the cooling rate than others [Liu et al., 2018]. It should also be noted that certain glass properties or structural features (e.g., medium-range order structure) are more sensitive to the cooling rate than others (e.g., short-range order structure) [Li et al., 2017].

### 3.3. Finite size effects

Due to their high computational cost, atomistic simulations are limited to fairly small systems (i.e., small number of atoms). Although PBC are typically used to mitigate any spurious effects arising from the presence of surfaces, the limited size of simulated glasses (from hundreds to millions of atoms) can affect the



**Figure 9.** (a) Illustration of different local minimum states in the potential energy landscape (PEL) that are reached by melt-quenched glasses upon different cooling rates [Debenedetti and Stillinger, 2001]. Slower cooling rates result in more stable glasses, i.e., featuring a deeper position in the PEL. (b) Evolution of the potential energy  $U$  of a glass with respect to temperature during a melt-quenching molecular dynamics (MD) simulation under fast cooling (yellow) and slow cooling (blue) [Debenedetti and Stillinger, 2001]. The energy profile of a glass subjected to a melt-quenching experiment (i.e., at much lower cooling rate) is added as a reference (green). (c) Fictive temperature  $T_f$  (upper panel) and final potential energy  $U_0$  (bottom panel) as a function of cooling rate for a  $(\text{Na}_2\text{O})_{30}(\text{SiO}_2)_{70}$  glass offered by both melt-quenching MD simulations (blue squares) and experiments (green squares) [Li et al., 2017, Zhou et al., 2020]. The lines are to guide the eyes.

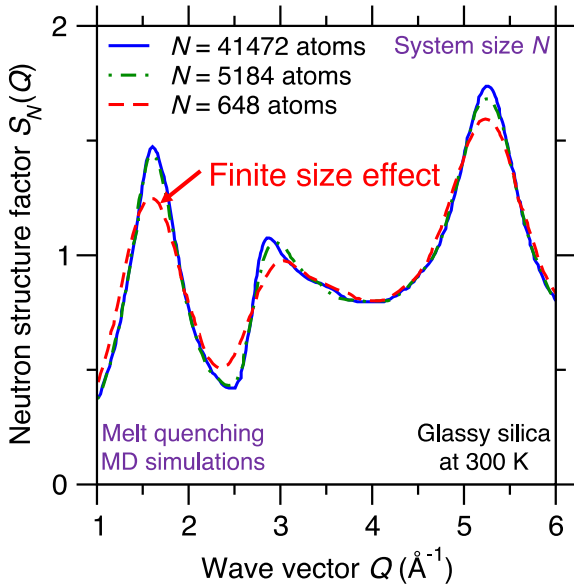


**Figure 10.** Neutron structure factor  $S_N(Q)$  of silica glasses prepared by melt-quenching molecular dynamics (MD) simulations for varying system sizes, namely,  $N = 648$ ,  $5184$ , and  $41,472$  atoms [Nakano et al., 1994].

accuracy of the simulation [Du, 2015]. Difficulties related to the system size include: (i) lack of statistical sampling if the number of atoms is too low [Berthier et al., 2012, Horbach et al., 1996], (ii) enhanced fluctuations in the thermodynamic properties of the simulated system (e.g., temperature or pressure) since the magnitude of fluctuations inversely scale with the square root of the number of atoms [Du, 2019, Leach, 2001], and (iii) systematic errors arising from the limited size of the simulation box (e.g., absence of large rings or extended collective vibrational modes) [Ganster et al., 2004, Nakano et al., 1994].

Figure 10 shows the computed neutron structure factor  $S_N(Q)$  of a glassy silica system prepared by melt-quenching MD simulations while using three different system sizes  $N$ , namely, 648 (small system), 5184 (intermediate system), and 41,472 atoms (large system) [Nakano et al., 1994]. The computed structure factor  $S_N(Q)$  is found to depend on the system size since, especially in the low- $Q$  region (which captures the medium-range order structure of the glass)—before the structure factor eventually converges for large systems [Nakano et al., 1994]. This indicates that glass simulations relying on small simulation boxes (and, hence, small numbers of atoms)

do not always properly capture the structure and properties of glasses [Du, 2015, Ganster et al., 2004, Nakano et al., 1994]. In practice, one needs to select a system size that is large enough to mitigate finite size effects, but small enough to ensure a reasonable computational cost [Du, 2015].

### 3.4. Limitations of reverse Monte Carlo (RMC) simulations

#### 3.4.1. Need for structural data

Reverse Monte Carlo (RMC) simulations aim to construct atomistic structures that match one or several structural fingerprints provided by experiments (often, the PDF) [McGreevy, 2001]. As such, RMC simulations offer an attractive alternative to MD simulations since such simulations can effectively bypass the melt-quench route to form a glass and, hence, are not affected by high cooling rate effects. However, RMC simulations largely rely on the availability (and accuracy) of experimental data. This limits the predictive power of RMC simulations since this approach does not make it possible to simulate *in silico* glasses that have not been experimentally synthesized and characterized yet. This also limits the range of conditions (temperature, pressure, etc.) to the ones that have already been experimentally explored.

#### 3.4.2. Ill-defined nature of RMC simulations

RMC simulations adopt the MC algorithm to search for an atomic structure that exhibits a minimum in the cost function landscape (see upper panel of Figure 11a) [Allen and Tildesley, 2017], wherein the cost function  $R_\chi$  is defined as the magnitude of difference between the simulated structural fingerprints and their experimental references [Zhou et al., 2020]. This can be formulated as an optimization problem, wherein some degrees of freedom (i.e., the positions of the atoms) are adjusted so as to minimize a cost function. However, the optimization problem at the core of RMC simulations is intrinsically ill-defined. Indeed, although a given three-dimensional structure yields unique values for the fingerprints, a given fingerprint can be associated with a large number of different three-dimensional structures. That is, the structure–fingerprint relationship is not reversible.

For instance, due to the complex, disordered nature of glasses [Bunde and Havlin, 2012], very different structures can be associated with the same PDF (see Figure 11b) [Pandey et al., 2016b]. This is a consequence of the fact that the PDF is simply a one-dimensional signature of a glass structure (averaged over various types of elements) and, therefore, only offers a highly compressed representation of a three-dimensional structure—which does not contain enough information to robustly reconstruct the structure itself. In short, RMC simulations do not exhibit a single solution, which manifests itself by the fact that the cost function landscape exhibits various competitive minima [Pandey et al., 2015]. Since traditional RMC simulations do not embed any knowledge of the interatomic interactions, the structures generated by RMC may not be thermodynamically stable [Zhou et al., 2020] and the regions of the PEL that are explored in RMC simulations may be very different from those that are accessed during the melt-quenching of a glass (see bottom panel in Figure 11a) [Pandey et al., 2015].

Figure 11c shows the evolution of the optimization cost function  $R_\chi$  and the potential  $U$  with respect to the number of MC search steps during an RMC simulation for a  $(\text{Na}_2\text{O})_{30}(\text{SiO}_2)_{70}$  glass [Zhou et al., 2020]. Note that the values of  $R_\chi$  and  $U$  obtained for the same glass prepared by a melt-quenching MD simulation are also added as references [Zhou et al., 2020]. As expected,  $R_\chi$  gradually decreases and eventually becomes lower than the MD reference, that is, the RMC simulation offers an optimal structure that indeed matches the experimental structural fingerprints (see upper panel of Figure 11c) [Zhou et al., 2020]. However, upon RMC refinement, the potential energy  $U$  is not monotonically decreasing but, rather, tends to increase in the late stages of the MC search. Eventually, the final glass structure exhibits a notably higher potential energy  $U$  than that of the MD-simulated glass reference (see bottom panel of Figure 11c) [Zhou et al., 2020]. These results exemplify that an apparent excellent agreement with experimental data (e.g., based on the PDF) does not always translate into a realistic glass structure [Pandey et al., 2015, Zhou et al., 2020]. The ill-defined nature of RMC can be partially mitigated by the introduction of an energy penalty term  $U$  in the MC cost function to favor structures featuring low potential energy—an approach that is typically referred



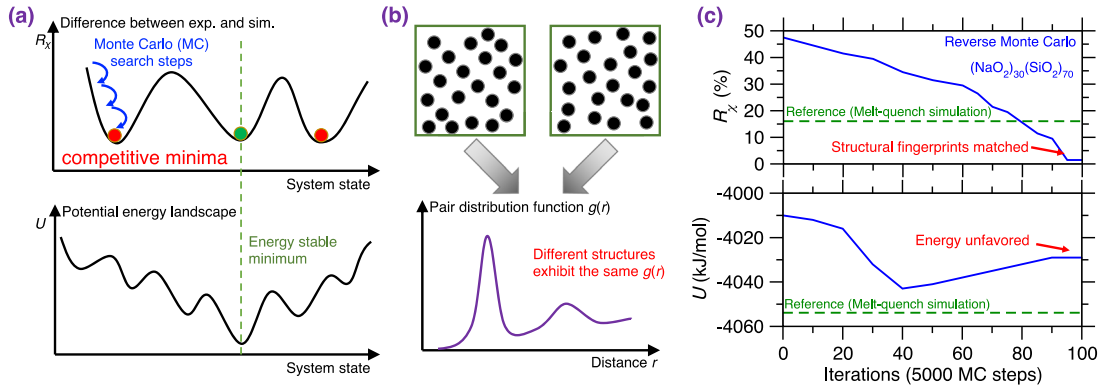


**Figure 11.** (a) Illustration of the existence of competitive minima in the cost function landscape for a reverse Monte Carlo (RMC) simulation [McGreevy, 2001]. The cost function  $R_\chi$  is defined herein as the magnitude of difference between the simulated and experimental PDFs (see (1)) [Zhou et al., 2020]. Compared to the targeted minimum (green circle, which exhibits both low  $R_\chi$  and potential energy  $U$ ), some competitive minima (red sphere) exhibit the same value of the cost function  $R_\chi$ , but high values of  $U$ , i.e., they correspond to unstable energy states in the potential energy landscape (PEL) [Zhou et al., 2020]. (b) Illustration of atomic configurations that exhibit the same PDF  $g(r)$  while presenting notably different structures [Pandey et al., 2016b]. (c) Evolution of the cost function  $R_\chi$  (upper panel) and potential energy  $U$  (bottom panel) as a function of the number of Monte Carlo (MC) search steps during an RMC simulation of a sodium silicate glass ((NaO<sub>2</sub>)<sub>30</sub>(SiO<sub>2</sub>)<sub>70</sub>) [Zhou et al., 2020]. The  $R_\chi$  and  $U$  values obtained for the same glass prepared by melt-quenching molecular dynamics (MD) simulation with a cooling rate of 0.001 K/ps are added as references (green dash line) [Zhou et al., 2020].

to as hybrid RMC [Bousige et al., 2015, Jain et al., 2006, Opletal et al., 2002]. However, hybrid RMC requires trial-and-error tests or intuition to adjust the weights of  $R_\chi$  and  $U$  in the cost function. In addition, hybrid RMC simulations are significantly more computationally expensive than traditional RMC simulations since the potential energy of the system  $U$  must be computed at each MC step [Zhou et al., 2020].

## 4. New developments in atomistic modeling of glasses

### 4.1. Machine-learned forcefields

#### 4.1.1. Types of machine-learned forcefields

To address the limitations associated with empirical forcefields relying on a fixed analytical form, machine learning (ML) offers a promising pathway to develop new complex forcefields that rely on an ML model to map a given atomic configuration to its potential energy. The promise of machine-learned

forcefields is to approach the accuracy of *ab initio* simulations with a computational burden that is more comparable to (although typically higher than) that of classical empirical forcefields. In detail, machine-learned forcefields adopt ML regression models to fit the system's PEL as a function of the atom positions [Behler, 2016, Mishin, 2021, Mueller et al., 2020], without the need to rely on any physical or chemical intuition to define a functional format of the empirical forcefield [Du, 2015, Huang and Kieffer, 2015]. The ground-truth PEL datapoints are often provided by *ab initio* MD simulations [Boero et al., 2015]. Several types of regression models have been developed so far to interpolate the PEL information provided by *ab initio* simulations [Mishin, 2021], i.e., to map the system's atom positions  $\{r_i\}$  to its potential energy  $U\{r_i\}$  (see Figure 12a). This includes (i) physically informed neural networks (PINN) or PINN-type regression models, which use as inputs several structural features (e.g., translation- and rotation-invariant angular 3-body and radial 2-body order parameters [Bartók et al., 2013, Chmiela



*et al.*, 2018, Pun *et al.*, 2019]) to predict the system's potential energy  $U$  [Huan *et al.*, 2017, Pun *et al.*, 2019, Schütt *et al.*, 2018], (ii) graph neural networks (GNN), which directly use as input the atom positions (modeled as a graph, wherein some nodes, the atoms, are connected by some edges, the chemical interactions) to predict  $U$  [Gilmer *et al.*, 2017, Park *et al.*, 2021], and (iii) Gaussian approximation potentials (GAP), which, in contrast to the neural network fitting used in PINN and GNN [Russell *et al.*, 2010], adopt a nonparametric fitting technique (i.e., Gaussian process regression (GPR) [Rasmussen and Williams, 2008]) to offer not only the PEL prediction but also the confidence interval of the prediction [Bartók *et al.*, 2010, Bartók and Csányi, 2015]. Importantly, this confidence interval can be used to train forcefields by active learning, that is, wherein new ground-truth *ab initio* simulations are dynamically conducted for structures associated with high confidence intervals—which are then added to the training set to retrain the GAP forcefield. Such active learning makes it possible to dynamically retrain the forcefield based on the very structures that are the most informative to improve its accuracy [Byggmästar *et al.*, 2019, Caro, 2019].

#### 4.1.2. Accuracy of machine-learned forcefields

As compared to empirical forcefields based on fixed functional formats [Du, 2019], machine-learned forcefields exhibit more flexibility to fit the PEL and, therefore, tend to offer more accurate predictions (when properly trained) [Mishin, 2021]. Figure 12b illustrates, from the viewpoint of a PEL [Lacks, 2001], the amorphous-to-crystalline transition of a silicon solid upon increasing pressure [McMillan *et al.*, 2005, Pandey *et al.*, 2011]. The reference PEL datapoints are provided by *ab initio* MD simulations and are fitted by both an analytical classical and a machine-learned forcefield, respectively [Deringer *et al.*, 2021]. The evolution of the average atomic volume as a function of pressure predicted by both the classical and machine-learned forcefields are provided in Figure 12c [Deringer *et al.*, 2021]. On the one hand, the classical forcefield based on a SW potential offers a good description of the close-to-equilibrium states (amorphous and crystalline states, corresponding to local minima in the PEL) [Stillinger and Weber, 1985], but fails to properly predict the pressure-driven amorphous-to-crystalline transition

[Deringer *et al.*, 2021] as it overestimates the energy barrier between these two states [Debenedetti and Stillinger, 2001]. On the other hand, the GAP machine-learned forcefield accurately fits the reference PEL datapoints and offers an accurate prediction of the energy of the transition state upon increasing pressure [Deringer *et al.*, 2021]. This illustrates the ability of machine-learned forcefields to offer accurate predictions, both for equilibrium and out-of-equilibrium systems [Mishin, 2021]. It should nevertheless be noted that, like any ML model, the accuracy of a machine-learned forcefield largely depends on the size, accuracy, and diversity of the training set—that is, the ensemble of configurations (and their ground-truth potential energy) that are used to train the forcefield.

As an emerging family of forcefields [Chmiela *et al.*, 2018], machine-learned forcefields have been successfully applied to simulate select glasses or disordered solids [Friederich *et al.*, 2021], including amorphous Si [Deringer *et al.*, 2021], silica [Li and Ando, 2018], Ge–Sb–Te (GST) phase-change materials [Mocanu *et al.*, 2020, 2018], MOFs [Eckhoff and Behler, 2019], etc. On the one hand, these forcefields yield very accurate predictions, whose accuracy approaches that of *ab initio* MD [Chmiela *et al.*, 2018]. On the other hand, in contrast to the high computation cost of *ab initio* MD [Hafner, 2008], the MD simulations relying on machine-learned forcefields are more efficient, which unlocks the prediction of more complex properties—e.g., properties involving long-term timescales or extended length scales [Friederich *et al.*, 2021], such as thermal conductivity [Sosso *et al.*, 2018], glass reactivity [Erlebach *et al.*, 2021], and phase transformations [Deringer *et al.*, 2021]. Clearly, machine-learned forcefields are an extremely promising pathway to address the challenges facing the simulation of glasses, but their challenging parameterization remains a key bottleneck.

#### 4.2. Development of analytical empirical forcefields by machine learning

##### 4.2.1. Advantages of analytical empirical forcefields

Despite the fact that, thanks to their flexibility, machine-learned forcefields have the potential to offer very high accuracy [Mishin, 2021], analytical empirical forcefields exhibit several key advantages

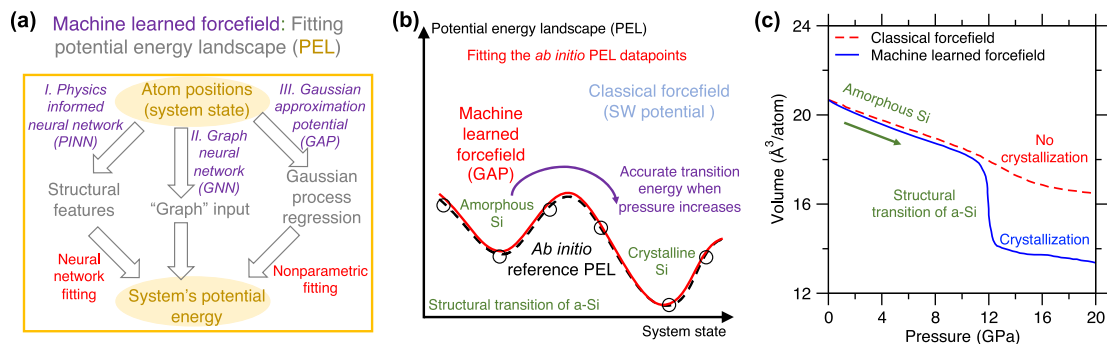


**Figure 12.** (a) Schematic illustrating various methods to obtain a machine-learned forcefield by fitting the potential energy landscape (PEL) of a system through (i) physically informed neural network (PINN) [Pun et al., 2019], (ii) graph neural network (GNN) [Park et al., 2021], (iii) Gaussian approximation potential (GAP) (see text for details) [Bartók et al., 2010]. In the fitting process, the reference PEL datapoints are provided by *ab initio* molecular dynamics (MD) simulations [Boero et al., 2015]. (b) Example of the structural transition of amorphous silicon (a-Si) into crystalline Si when pressure increases [McMillan et al., 2005, Pandey et al., 2011], by using MD simulations relying on a machine-learned forcefield [Deringer et al., 2021]. The transition process is illustrated in terms of a PEL computed by first-principles calculation (i.e., *ab initio* reference [Boero et al., 2015]), machine-learned forcefield (i.e. GAP [Deringer et al., 2021]), and classical forcefield (i.e., SW potential [Stillinger and Weber, 1985]), respectively. The GAP forcefield is trained by fitting the *ab initio* PEL datapoints (black circle) and exhibits a more accurate prediction of the transition energy of silicon upon crystallization than the classical forcefield [Deringer et al., 2021]. (c) Evolution of the average atomic volume as a function of the silicon system’s pressure using classical (i.e., SW potential [Stillinger and Weber, 1985]) and machine-learned forcefields (i.e., GAP [Deringer et al., 2021]). A crystallization transition is observed using GAP (as expected) but does not occur when using the SW potential [Deringer et al., 2021].

[Du, 2015, Huang and Kieffer, 2015]. As an important feature, the functional forms are selected based on physical and chemical knowledge/intuition regarding the nature of the interatomic interactions [van Beest et al., 1990]. For instance, ion-ion interactions are modeled based on the Coulomb’s law, forcefields can explicitly account for Van der Waals interactions (with a term proportional to  $1/r^6$ ), or the dipole of an atom can explicitly be modeled as a spring in polarizable forcefields [Allen and Tildesley, 2017, Carré et al., 2016, Du, 2015, Fennell and Gezelter, 2006, Huang and Kieffer, 2015, Musgraves et al., 2019]. This tends to render empirical forcefields more physics-based, but also more interpretable than their “black-box” machine-learned counterparts [Cranmer et al., 2020, Hernandez et al., 2019]. Such fixed analytical form also has several advantages. First, it imposes a strong constraint on the predicted potential energy—for instance, the selected analytical form can en-

sure that the energy diverges to infinity at close distance and converges to zero at long distance [Senftle et al., 2016]. This is important as, in contrast, due to their large flexibility, machine-learned forcefields can sometimes offer unrealistic, nonphysical predictions. This is a consequence of the fact, like any ML model, machine-learned forcefields can excel at interpolating the regions of the PEL that they have been trained on, but tend to offer very unrealistic predictions far from their training set. In turn, the fixed analytical form of analytical forcefields limit their ability to accurately interpolate complex PEL, but makes them more robust and more likely to offer reasonable transferability to systems that are different from those included in the training set [Liu et al., 2019c]. Second, machine-learned forcefields typically rely on complex models (e.g., artificial neural networks) that present a very large number of tunable parameters. Such a large dimensionality must be balanced by a

large training set. As a result, machine-learned forcefields typically require a significantly larger training set (that is, a larger number of configurations with their ground-truth potential energy) than analytical empirical forcefields (which typically involve orders of magnitude fewer parameters) [Liu et al., 2020a]. In addition, although machine-learned forcefields have the flexibility to interpolate any PEL without requiring any intuition regarding the nature of the interactions, they still rely on a certain number of assumptions regarding the complexity of the PEL (e.g., to determine the optimal number of neurons or layers in an artificial neural network model). Finally, although machine-learned forcefields are orders of magnitude faster than *ab initio* simulations, they still typically involve an increased computational burden as compared to simple analytical forcefields [Cranmer et al., 2020, Yaseen et al., 2016].

#### 4.2.2. *Machine-learning-aided parameterization scheme*

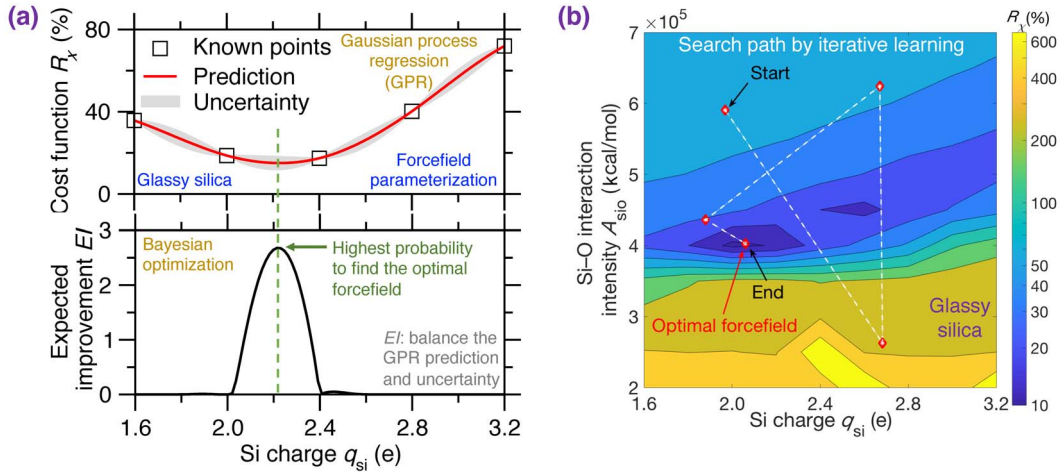
As an alternative to machine-learned forcefields, machine-learning-aided parameterization can combine the power of ML with the robustness of analytical forcefields. Indeed, as compared to traditional gradient-descent-based parameterization schemes (see Figure 8) [Carré et al., 2016], ML offers a new paradigm to parameterize analytical forcefields in a more efficient and unbiased fashion [Liu et al., 2019e]. For instance, Figure 13 shows an ML-aided parameterization scheme based on Gaussian process regression (GPR) and Bayesian optimization (BO) [Frazier and Wang, 2016, Ueno et al., 2016], which is applied to parameterize a Buckingham forcefield (see (5)) for glassy silica [Liu et al., 2019e]. The ML approach aims to find the global minimum (i.e., the optimal set of parameters) in the cost function landscape as a function of the forcefield parameters [Liu et al., 2019c], where the cost function  $R_\chi$  is here defined as the magnitude of difference of the PDF  $g(r)$  computed by classical MD simulation and its *ab initio* reference [Wright, 1993].

Figure 13a illustrates the basic idea behind the use of GPR and BO to parameterize empirical forcefields [Liu et al., 2019c]. For illustration purposes, only one forcefield parameter (i.e., silicon charge  $q_{\text{Si}}$ ) is here selected to plot the cost function landscape [Liu et al., 2019c], while the other parameters are fixed to their values in the well-established BKS potential

[van Beest et al., 1990]. First, the GPR model fits the known (i.e., ground-truth) points in the cost function landscape—so as to offer not only a smooth interpolation of the landscape profile but also its confidence interval (see upper panel of Figure 13a) [Liu et al., 2019c]. Then, BO prescribes the set of parameters (i.e.,  $q_{\text{Si}}$  herein) that exhibits the highest probability to yield the global minimum for  $R_\chi$  (see bottom panel of Figure 13a) [Liu et al., 2019c]. This is achieved by computing the expected improvement (EI) metric that offers the best balance between (i) the “exploitation” of the forcefields parameters that are predicted by the GPR model to yield a minimum  $R_\chi$  value and (ii) the “exploration” of the domains of forcefield parameter values that are associated with high confidence interval (i.e., high uncertainty) [Frazier and Wang, 2016]. This parameterization scheme ensures that the optimal forcefield parameters (i.e., those that minimize the cost function) can quickly be identified, while mitigating the risk for the optimization scheme to remain stuck in a local minimum of the cost function landscape.

#### 4.2.3. *Efficient search of global minimum*

Figure 13b shows the search path that is prescribed by ML to find the optimal forcefield parameters (i.e., those yielding a global minimum for the cost function  $R_\chi$ ) [Liu et al., 2019e]. For illustration purposes, the search is conducted within a two-dimensional parameter space (i.e., comprising the silicon partial charge  $q_{\text{Si}}$  and the short-range SiO interaction intensity  $A_{\text{SiO}}$ ) [Liu et al., 2019e], while the other forcefield parameters are fixed to their values in the BKS potential [van Beest et al., 1990]. Notably, this ML-aided parameterization approach can quickly identify the optimal set of forcefield parameters after only a few iterations [Liu et al., 2019e]. Importantly, this optimization scheme is unbiased to the start position in the search space, that is, the outcome of the optimization does not depend on the initial values of the forcefield parameters [Liu et al., 2019e]. This approach offers a promising route to efficiently refine existing empirical forcefields at a fraction of the computational cost that is needed to develop a machine-learned forcefield [Liu et al., 2020a, 2019c,e].



**Figure 13.** (a) Parameterization of a Buckingham-format empirical forcefield (see (5)) for glassy silica based on Gaussian process regression (GPR) and Bayesian optimization (BO) (see text for details) [Liu et al., 2019c]. For illustration purposes, only  $q_{\text{Si}}$  is set as a variable, while the other forcefield parameters are fixed to their values in the well-established van Beest–Kramer–van Santen (BKS) potential [van Beest et al., 1990]. (b) Illustration of the efficient search for optimal forcefield parameters (i.e., yielding minimum  $R_{\chi}$ ) for glassy silica in the parameter space of the Buckingham forcefield by the iterative learning method combining GPR and BO [Liu et al., 2019e]. For illustration purposes, a two-dimensional parameter space (i.e.,  $q_{\text{Si}}$  and  $A_{\text{SiO}}$ ) is adopted in the search process, while the other forcefield parameters are fixed to their values in the BKS potential [van Beest et al., 1990]. The search path (white dashed line) prescribed by ML quickly identifies the optimal forcefield after only five iterations [Liu et al., 2019e].

### 4.3. Constructing stable glass structures by force-enhanced atomic refinement

#### 4.3.1. Bypassing the melt-quenching route

Due to the huge gap of cooling rate between melt-quenching experiments and MD simulations (see Figure 9) [Li et al., 2017], glasses prepared by MD simulations tend to exhibit higher fictive temperature (i.e., to be less stable) than experimentally synthesized glasses [Vollmayr et al., 1996b]. Alternatively, RMC simulations can bypass this melt-quenching route by directly constructing atomic structures that match experimental data (see Section 2.2) [McGreevy, 2001]. However, due to the ill-defined nature of RMC (see Section 3.4), RMC-based glasses are often thermodynamically unstable (see Figure 11) [Pandey et al., 2015, Zhou et al., 2020]. To mitigate this issue, force-enhanced atomic refinement (FEAR) has been proposed as a powerful, information-based approach that simultaneously leverages the knowledge of experimental data (which

are used to constraint the glass structure) and inter-atomic potential (which is used to ensure the thermodynamic stability of the simulated glass) [Pandey et al., 2016a,b, 2015].

#### 4.3.2. FEAR algorithm

Figure 14a illustrates how the FEAR algorithm searches for a realistic atomistic structure that simultaneously matches experimental data and features minimum potential energy [Pandey et al., 2016a, 2015]. In detail, each FEAR iteration consists of a given number (e.g., 5000) of RMC search steps in the cost function landscape  $R_{\chi}$  (i.e., difference between simulated and experimental data), followed by one energy minimization step in the PEL [Zhou et al., 2020]. The cost function  $R_{\chi}$  is defined herein as the magnitude of the difference between the PDFs  $g(r)$  computed by FEAR simulation and neutron diffraction experiment [Zhou et al., 2020]. RMC and energy minimization steps are then iteratively repeated until both the cost function  $R_{\chi}$  and the potential energy converge. In this scheme, the RMC steps are

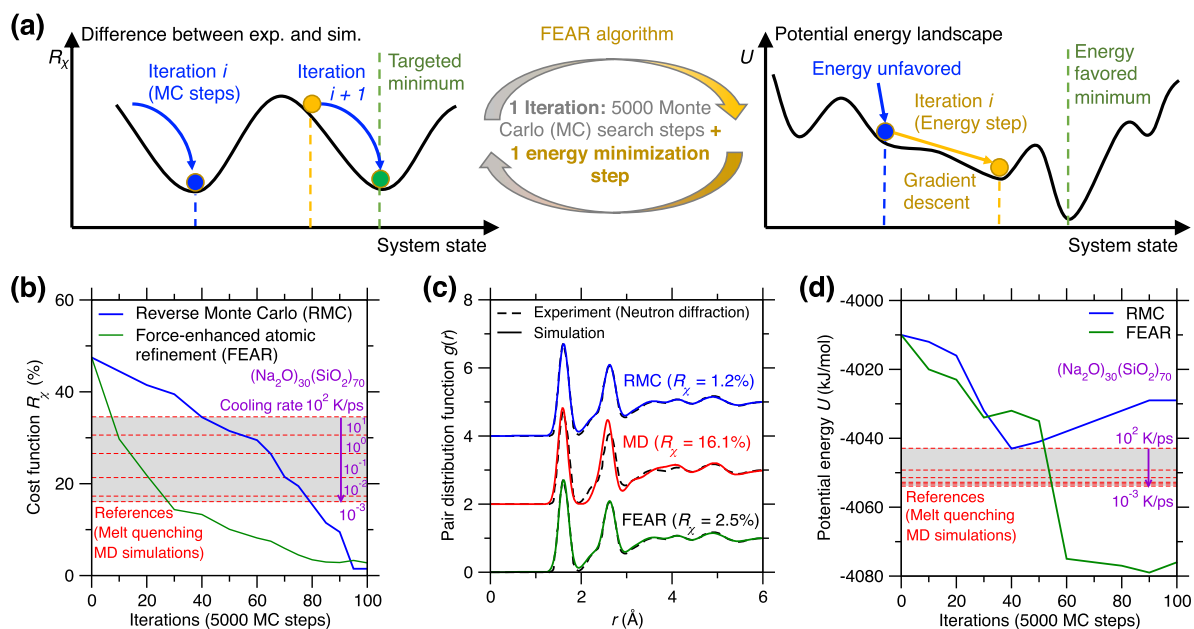


**Figure 14.** (a) Illustration of the force-enhanced atomic refinement (FEAR) algorithm, which combines both Monte Carlo (MC) searches in the cost function landscape—i.e., reverse Monte Carlo (RMC) simulation [McGreevy and Pusztai, 1988]—and energy minimization in the potential energy landscape (PEL) (see text for details) [Pandey *et al.*, 2015]. (b) Evolution of the cost function  $R_\chi$  (see (1)) as a function of the number of optimization iterations upon RMC (blue) and FEAR simulation (green) of a sodium silicate glass  $(\text{Na}_2\text{O})_{30}(\text{SiO}_2)_{70}$  [Zhou *et al.*, 2020]. The cost function  $R_\chi$  of glasses prepared by melt-quenching molecular dynamics (MD) simulations at different cooling rates ranging from  $10^2$  K/ps to  $10^{-3}$  K/ps are added as references (red dash lines) [Zhou *et al.*, 2020]. (c) Pair distribution function (PDF)  $g(r)$  of the glasses formed at the end of the RMC, MD, and FEAR simulation [Zhou *et al.*, 2020], compared to the  $g(r)$  reference obtained by neutron diffraction experiment [Wright *et al.*, 1991]. (d) Evolution of the system's potential energy  $U$  as a function of the number of optimization iterations upon RMC (blue) and FEAR simulation (green) [Zhou *et al.*, 2020]. The potential energy of glasses prepared by melt-quenching MD simulations are also added as references (red dash lines) [Zhou *et al.*, 2020].

used to slightly deform the atomic structure (so as to escape local minima in the PEL), while the energy minimization is used to ensure that the simulated structure never drifts away from the stable region of the PEL that is physically accessible [Pandey *et al.*, 2015, Zhou *et al.*, 2020]. Eventually, by simultaneously leveraging both experimental and interatomic energy information, FEAR simulations can yield glass structures that simultaneously exhibit enhanced agreement with available experimental data and a larger thermodynamic stability than glasses prepared by MD or RMC [Pandey *et al.*, 2015]. It is worth pointing out that, in contrast to MD sim-

ulations that heavily rely on the accuracy of interatomic forcefields [Takada, 2021], the accuracy of FEAR simulation is fairly insensitive to the quality of interatomic forcefield that is used during the energy minimization step [Zhou *et al.*, 2021]. That is, both high- and low-quality forcefields can guide the system toward energy-stable regions in the PEL, while, eventually, the details of the simulated structure are mainly controlled by the RMC steps [Zhou *et al.*, 2021]. Importantly, FEAR simulations are extremely computationally efficient since the potential energy of the system only needs to be computed during the energy minimization step—whereas it needs to be

computed at any step during MD or hybrid RMC simulations.

#### 4.3.3. Realistic prediction of atomistic structure

Figure 14b shows the evolution of the cost function  $R_\chi$  as a function of the number of optimization steps for both RMC and FEAR simulations [Zhou et al., 2020]. The  $R_\chi$  values of glasses prepared by melt-quenching MD simulations at different cooling rate are added as references [Zhou et al., 2020]. Both FEAR and RMC eventually offer atomistic structures exhibiting small  $R_\chi$  values, which are notably lower than that of the MD references [Zhou et al., 2020]. Indeed, the PDFs  $g(r)$  provided by both FEAR and RMC simulations are in excellent agreement with the experimental  $g(r)$  (see Figure 14c) [Zhou et al., 2020], while MD simulation slightly deviates from the experimental  $g(r)$  due to the large cooling rate [Li et al., 2017]. Interestingly, the energy minimizations steps upon FEAR refinement yield a faster convergence (i.e., faster decrease in the cost function  $R_\chi$ ) as compared to RMC. Further, Figure 14d shows the evolution of the potential energy  $U$  as a function of the number of optimization steps both upon FEAR and RMC simulations [Zhou et al., 2020]. MD simulation results are also added as references [Zhou et al., 2020]. It is notable that RMC simulation yields unrealistic atomic structures that are unstable as they present a potential energy that is significantly higher than those achieved by MD [Zhou et al., 2020]. In comparison, the FEAR simulation offers a notably more realistic, energy-stable atomistic structure that still satisfies the experimental constraints as well as the RMC-based structure [Zhou et al., 2020]. Importantly, the FEAR-generated structure features a potential energy that is notably lower than those achieved by melt-quenching MD, even in the case of the slowest cooling rate [Zhou et al., 2020]. This highlights the fact that the structure generated by FEAR exhibits a lower fictive temperature than the MD-based configurations—that is, FEAR can efficiently bypass limitations arising from the fast cooling rate used in MD simulations [Debenedetti and Stillinger, 2001, Li et al., 2017]. This establishes FEAR as a promising technique to generate glass structures that are very stable and that can directly be quantitatively compared with experimental glasses.

## 5. Conclusions and future opportunities

Overall, atomistic simulations provide an efficient tool to access the atomic structure of glasses, which is otherwise challenging to directly visualize by conventional experiments. However, simulations remain plagued by a series of challenges, including (i) slow execution runtime, (ii) small accessible timescales and/or length scales, (iii) cooling rate difference between experiments and simulations, (iv) availability and accuracy of empirical forcefields, and (v) ill-defined nature of simulation protocols (e.g., RMC simulations). To overcome these limitations, one can resort to either (i) simulation protocols involving more physical information (e.g., FEAR simulations, or more accurate empirical forcefield functionals) or (ii) ML approaches (e.g., machine-learned forcefields, or ML-aided forcefield parameterization). Indeed, with the aid of ML, one can develop more accurate and computationally efficient forcefields to speed up MD simulations, thereby unlocking longer timescales or larger system sizes.

As a future opportunity, we envision that smart closed-loop integrations of ML modeling and MD simulations will leapfrog glass modeling (see Figure 15). Example of such opportunities are listed in the following:

(i) *Deciphering complex simulation data by ML.* Atomic trajectories generated by MD simulations contains all the structural information that govern glass properties. However, due to the complex, disordered nature of glass structures, it is challenging to “separate the wheat from the chaff”, that is, to pinpoint the key structural features that govern glass properties [Tanaka et al., 2019]. In that regard, owing to its ability to discover hidden pattern in complex, multi-dimensional data, ML offers a new opportunity to identify relevant structural patterns in simulated glassy structures [Biroli, 2020, Tanaka et al., 2019]. Prominent examples include the recently developed softness approach based on classification-based ML [Cubuk et al., 2017, Liu et al., 2021c,b] and graph neural networks (GNN)—a new and powerful family of ML models—that represent atomistic structures as nodes-and-edges graphs [Bapst et al., 2020]. Inputting complex simulation data into such advanced ML models makes it possible to decipher previously hidden structure–property relationships

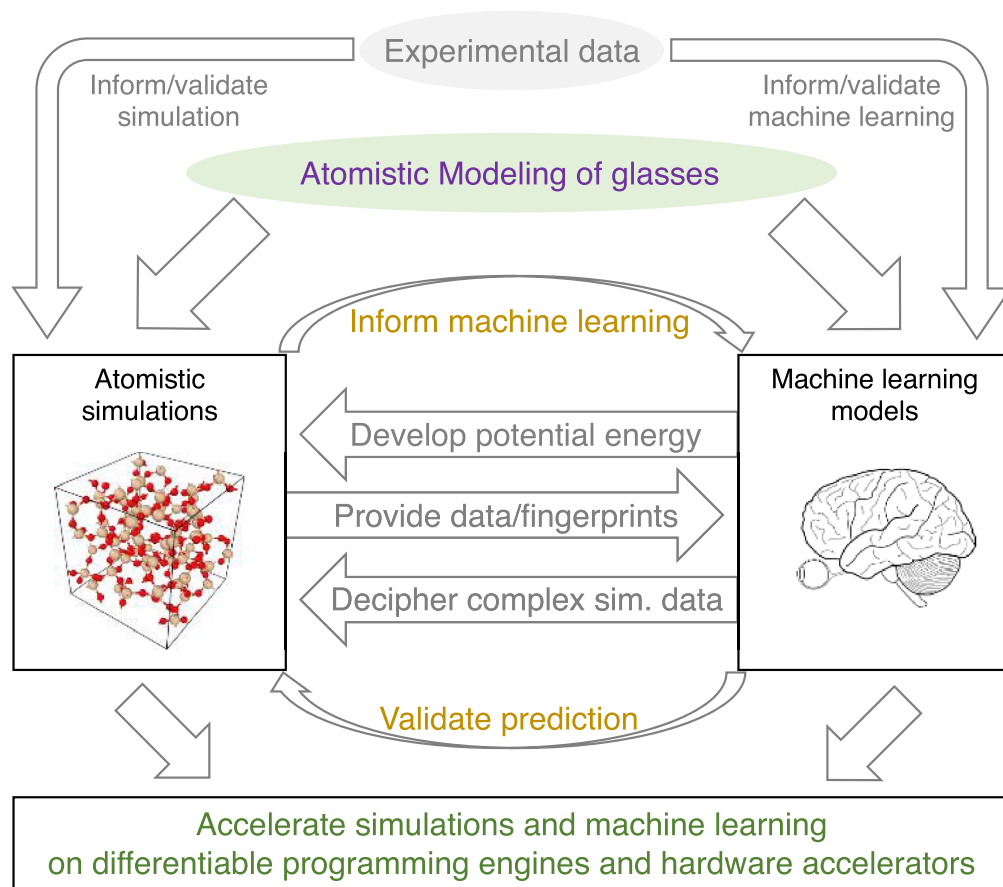


**Figure 15.** Schematic summarizing future opportunities for glass modeling offered by the mutual integration of simulations and machine learning (ML). On the one hand, ML can assist in (i) developing empirical forcefields for accurate and computationally efficient simulations [Liu et al., 2019e], (ii) “separating the wheat from the chaff” in large amounts of complex simulation data to gain new insights or generate new knowledge of the underlying physics governing glasses [Liu et al., 2021b], and (iii) accelerating simulations by surrogate ML engines [Liu et al., 2021a]. On the other hand, simulation can generate large amounts of high-fidelity data that can be used to train ML models [Liu et al., 2019d], which, in turn, can be validated by simulations. Both simulations and their integration pipeline with ML can be accelerated by leveraging automated differentiable programming engines (e.g., Python JAX) and hardware accelerators (e.g., graphics processing unit (GPU) and tensor processing unit (TPU)) [Liu et al., 2020b]. Note that, when applicable, “ground-truth” experimental data can either *a priori* inform or *a posteriori* validate the physics-based (i.e., simulations) and data-based (i.e., ML) models.

and capture the key structural features that govern glass properties. The ability to learn new physics from ML models depends on their “interpretability”. For instance, one can analyze the weight associated to each input structural feature in the softness approach [Cubuk et al., 2017, Liu et al., 2021c,b] or monitor the model responses for various graph in-

puts in the GNN method [Bapst et al., 2020]. These approaches make it possible to unravel the key structural patterns, that is, the ones that are the most influential in governing the properties of glasses. Finally, it is worth mentioning that, in addition to ML, topological analyzes represent an alternative, traditionally challenging but direct approach to in-



investigate simulated glassy structures [Bauchy, 2019]. For instance, some recently developed topological approaches (e.g., persistent homology [Nakamura *et al.*, 2015]) have been demonstrated to be effective tools in identifying influential medium-range order structural features in disordered phases [Sørensen *et al.*, 2020].

*(ii) Combining simulations and ML for glasses' inverse design.* Owing to its economical nature as compared to systematic experiments, high-throughput virtual screening (HTVS, that is, the systematic simulation of a large number of glasses) offers an efficient route to identify *in silico* an optimal glass composition featuring an optimal characteristics within a given compositional domain [Noh *et al.*, 2020, Sanchez-Lengeling and Aspuru-Guzik, 2018]. However, although simulations excel at predicting the properties of a given glass as a function of its composition (i.e., “forward prediction”), their application to “inverse design” problems (that is, given an optimal property target, find the best glass composition) remains limited by their high computational cost—which prevents the systematic exploration of large compositional spaces [Sanchez-Lengeling and Aspuru-Guzik, 2018]. To address this issue, ML offers an ideal companion to MD simulations—since an ML model can learn from a series of MD simulations and, based on this, recommend what should be the next glass composition to simulate. Such closed-loop integrations of MD and ML could greatly accelerate the discovery of novel glasses featuring desirable properties or functionalities [Liu *et al.*, 2020b, 2019g, Noh *et al.*, 2020]. Note that, when applicable, it is desirable to integrate experimental data into the closed loop of MD and ML, wherein such “ground-truth” experimental data can either inform or validate the models (see Figure 15). This is essential to ensure the reliability of glass modeling approaches so as to avoid any “bubble effect” arising from the error accumulation within the closed-loop integration of MD and ML (wherein MD and ML would mutually comfort and amplify each other in their improper predictions) [Bagnoli *et al.*, 2022, Yang *et al.*, 2019b].

*(iii) Leveraging differentiable programming platforms.* When integrating simulations and ML models within unified pipelines, different programming languages can present a communication barrier between ML

and simulation packages, which often rely on Python and C++/Fortran, respectively. In addition, most MD packages are still rooted in fairly ancient computing paradigms (e.g., with no automated differentiation), which is reminiscent of the state of ML before automatic hardware acceleration and differentiation became popular. To overcome these frictions, automatic differentiable (auto-diff) programming platforms (e.g., Python JAX [Bradbury *et al.*, 2018]) have been recently developed to seamlessly integrate ML and simulations within unified pipelines. In contrast to traditional programming platforms that rely on handwritten derivatives (e.g., C++ [Plimpton, 1995b]), auto-diff platforms excel at computing on-the-fly the backward gradient of any quantities with no additional computation burden associated with differentiation [Bradbury *et al.*, 2018]—an operation that comes with a notable computing time in traditional simulators (e.g., force calculation in MD simulations [Allen and Tildesley, 2017], see Figure 4a). Moreover, simulations built on auto-diff platforms gain backward differentiability, which makes it possible to use their outcomes to directly train ML models using gradient back propagation [Schoenholz and Cubuk, 2020]. This create new opportunities to train a ML model directly based on differentiable physical knowledge rather than on data [Liu *et al.*, 2020b]. Finally, the auto-diff platforms generally enable native “just-in-time” compilation on high-performance dedicated hardware accelerators [Bradbury *et al.*, 2018, Schoenholz and Cubuk, 2020], such as graphics processing units (GPU) and tensor processing units (TPU) [Wang *et al.*, 2019]. Specifically, TPUs are specifically designed as matrix processors and, thanks to their tailored architecture, offer unparalleled performances in deep learning problems (up to 200X faster than GPUs). Note that MD simulations (e.g., JAX-MD [Schoenholz and Cubuk, 2020]) can natively run on GPU- or TPU-based auto-diff platforms, which is key to avoid any speed bottleneck arising due to moving from one hardware to another within simulation pipelines [Plimpton, 1995b, Schoenholz and Cubuk, 2020]. This could greatly accelerate MD simulations relying on artificial neural networks potentials [Liu *et al.*, 2020b, Yang *et al.*, 2019a].

*(iv) Replacing slow simulations by faster surrogate ML simulation engines.* Although the development of auto-diff platforms enables differentiable



simulations and native hardware acceleration, the computational efficiency of numerical simulations is still limited by the intrinsic computation cost associated with the underlying numerical algorithms (e.g., Newton's law of motion in MD simulations [Allen and Tildesley, 2017]). The numerical algorithms behind scientific numerical simulations are likely to remain their bottleneck [Lane, 2015, Yang et al., 2019b]. To mitigate this issue, surrogate ML simulation engines offer a unique, largely untapped opportunity to replace slow simulations so as to accelerate their execution without compromising accuracy [Kochkov et al., 2021, Liu et al., 2021a]. Surrogate ML engines can be implemented as artificial neural network (ANN) models, such as convolutional neural network (CNN) [Kochkov et al., 2021] or GNN [Bapst et al., 2020].

Overall, we envision that the “fusion” of experiments, simulations, and ML models (see Figure 15) will unlock a new era in glass modeling (and materials modeling in general)—wherein traditional boundaries between physics and empirical models, knowledge and data, forward and inverse predictions, or experimental and simulation data would eventually fade. We hope that the present perspective will modestly contribute to stimulating new developments in that direction.

## Conflicts of interest

Authors have no conflict of interest to declare.

## Acknowledgments

This work was supported by the National Science Foundation under Grants No. CMMI-1762292, CMMI-1826420, DMR-1928538, DMREF-1922167, and CAREER-1944510. Part of this work was also supported by the Department of Energy's Nuclear Energy University Program (DOE-NEUP: DE-NE18-15020).

## References

- Affatigato, M. (2015). *Modern Glass Characterization*. John Wiley & Sons, Hoboken, NJ.
- Alder, B. J. and Wainwright, T. E. (1959). Studies in molecular dynamics. I. General method. *J. Chem. Phys.*, 31, 459–466.
- Alder, B. J. and Wainwright, T. E. (1960). Studies in molecular dynamics. II. Behavior of a small number of elastic spheres. *J. Chem. Phys.*, 33, 1439–1451.
- Allen, M. P. and Tildesley, D. J. (2017). *Computer Simulation of Liquids*. Oxford University Press, New York.
- Almeida, R. M. and Santos, L. F. (2015). Raman spectroscopy of glasses. In *Modern Glass Characterization*, pages 1–33. John Wiley & Sons, Ltd, Hoboken, NJ.
- Andersen, H. C. (1980). Molecular dynamics simulations at constant pressure and/or temperature. *J. Chem. Phys.*, 72, 2384–2393.
- Arceri, F., Landes, F. P., Berthier, L., and Biroli, G. (2020). Glasses and aging: A statistical mechanics perspective. (cond-mat.stat-mech).
- Bachelet, G. B., Hamann, D. R., and Schlüter, M. (1982). Pseudopotentials that work: from H to Pu. *Phys. Rev. B*, 26, 4199–4228.
- Bagnoli, F., de Bonfioli Cavalcabo, G., Casu, B., and Guazzini, A. (2022). Bubble effect induced by recommendation systems in a simple social media model. In Benito, R. M., Cherifi, C., Cherifi, H., Moro, E., Rocha, L. M., and Sales-Pardo, M., editors, *Complex Networks & Their Applications X, Studies in Computational Intelligence*, pages 124–131. Springer International Publishing, Cham.
- Bapst, V., Keck, T., Grabska-Barwińska, A., Donner, C., Cubuk, E. D., Schoenholz, S. S., Obika, A., Nelson, A. W. R., Back, T., Hassabis, D., and Kohli, P. (2020). Unveiling the predictive power of static structure in glassy systems. *Nat. Phys.*, 16, 448–454.
- Baral, K., Li, A., and Ching, W.-Y. (2017). Ab initio modeling of structure and properties of single and mixed alkali silicate glasses. *J. Phys. Chem. A*, 121, 7697–7708.
- Bartók, A. P. and Csányi, G. (2015). Gaussian approximation potentials: A brief tutorial introduction. *Int. J. Quantum Chem.*, 115, 1051–1057.
- Bartók, A. P., Kondor, R., and Csányi, G. (2013). On representing chemical environments. *Phys. Rev. B*, 87, article no. 184115.
- Bartók, A. P., Payne, M. C., Kondor, R., and Csányi, G. (2010). Gaussian approximation potentials: the accuracy of quantum mechanics, without the electrons. *Phys. Rev. Lett.*, 104, article no. 136403.
- Bauchy, M. (2012). Structural, vibrational, and thermal properties of densified silicates: Insights from

- molecular dynamics. *J. Chem. Phys.*, 137, article no. 044510.
- Bauchy, M. (2014). Structural, vibrational, and elastic properties of a calcium aluminosilicate glass from molecular dynamics simulations: The role of the potential. *J. Chem. Phys.*, 141, article no. 024507.
- Bauchy, M. (2019). Deciphering the atomic genome of glasses by topological constraint theory and molecular dynamics: A review. *Comput. Mater. Sci.*, 159, 95–102.
- Bauchy, M., Guillot, B., Micoulaut, M., and Sator, N. (2013). Viscosity and viscosity anomalies of model silicates and magmas: a numerical investigation. *Chem. Geol.*, 346, 47–56. 9th Silicate Melts Workshop.
- Bauchy, M., Laubie, H., Abdolhosseini Qomi, M. J., Hoover, C. G., Ulm, F.-J., and Pellenq, R. J.-M. (2015). Fracture toughness of calcium–silicate–hydrate from molecular dynamics simulations. *J. Non Cryst. Solids*, 419, 58–64.
- Bauchy, M. and Micoulaut, M. (2011). From pockets to channels: density-controlled diffusion in sodium silicates. *Phys. Rev. B*, 83, article no. 184118.
- Bauchy, M. and Micoulaut, M. (2015). Densified network glasses and liquids with thermodynamically reversible and structurally adaptive behaviour. *Nat. Commun.*, 6, article no. 6398.
- Bauchy, M., Wang, B., Wang, M., Yu, Y., Abdolhosseini Qomi, M. J., Smedskjaer, M. M., Bichara, C., Ulm, F.-J., and Pellenq, R. (2016). Fracture toughness anomalies: viewpoint of topological constraint theory. *Acta Mater.*, 121, 234–239.
- Bauchy, M., Wang, M., Yu, Y., Wang, B., Krishnan, N. M. A., Masoero, E., Ulm, F.-J., and Pellenq, R. (2017). Topological control on the structural relaxation of atomic networks under stress. *Phys. Rev. Lett.*, 119, article no. 035502.
- Beake, E. O. R., Dove, M. T., Phillips, A. E., Keen, D. A., Tucker, M. G., Goodwin, A. L., Bennett, T. D., and Cheetham, A. K. (2013). Flexibility of zeolitic imidazolate framework structures studied by neutron total scattering and the reverse Monte Carlo method. *J. Phys. Condens. Matter*, 25, article no. 395403.
- Behler, J. (2016). Perspective: Machine learning potentials for atomistic simulations. *J. Chem. Phys.*, 145, article no. 170901.
- Berthier, L., Biroli, G., Coslovich, D., Kob, W., and Toninelli, C. (2012). Finite-size effects in the dynamics of glass-forming liquids. *Phys. Rev. E*, 86, article no. 031502.
- Berthier, L. and Ediger, M. D. (2020). How to “measure” a structural relaxation time that is too long to be measured? *J. Chem. Phys.*, 153, article no. 044501.
- Binder, K. and Kob, W. (2011). *Glassy Materials and Disordered Solids: An Introduction to Their Statistical Mechanics*. World Scientific, Singapore.
- Biroli, G. (2020). Machine learning glasses. *Nat. Phys.*, 16, 373–374.
- Biswas, P., Atta-Fynn, R., and Drabold, D. A. (2004). Reverse Monte Carlo modeling of amorphous silicon. *Phys. Rev. B*, 69, article no. 195207.
- Bitzek, E., Koskinen, P., Gähler, F., Moseler, M., and Gumbusch, P. (2006). Structural relaxation made simple. *Phys. Rev. Lett.*, 97, article no. 170201.
- Boero, M., Bouzid, A., Le Roux, S., Ozdamar, B., and Massobrio, C. (2015). First-principles molecular dynamics methods: an overview. In Massobrio, C., Du, J., Bernasconi, M., and Salmon, P. S., editors, *Molecular Dynamics Simulations of Disordered Materials, Springer Series in Materials Science*, pages 33–55. Springer International Publishing, Cham.
- Bottaro, S. and Lindorff-Larsen, K. (2018). Biophysical experiments and biomolecular simulations: a perfect match? *Science*, 361, 355–360.
- Bouhadja, M., Jakse, N., and Pasturel, A. (2013). Structural and dynamic properties of calcium aluminosilicate melts: a molecular dynamics study. *J. Chem. Phys.*, 138, article no. 224510.
- Bousige, C., Boğan, A., Ulm, F.-J., Pellenq, R. J.-M., and Coasne, B. (2015). Optimized molecular reconstruction procedure combining hybrid reverse Monte Carlo and molecular dynamics. *J. Chem. Phys.*, 142, article no. 114112.
- Bouty, O., Delaye, J. M., Beuneu, B., and Charpentier, T. (2014). Modelling borosilicate glasses of nuclear interest with the help of RMC, WAXS, neutron diffraction and 11B NMR. *J. Non Cryst. Solids*, 401, 27–31. STRUCTURE OF NON-CRYSTALLINE MATERIALS 12 Proceedings of the 12th International Conference on the Structure of Non-Crystalline Materials (NCM 12).
- Bradbury, J., Frostig, R., Hawkins, P., Johnson, M. J., Leary, C., Maclaurin, D., Nacula, G., Paszke, A., VanderPlas, J., Wanderman-Milne, S., and Zhang, Q. (2018). JAX: composable transformations of Python+NumPy programs. <http://github.com/>

- google/jax.
- Buehler, M. J., van Duin, A. C. T., and Goddard, W. A. (2006). Multiparadigm modeling of dynamical crack propagation in silicon using a reactive force field. *Phys. Rev. Lett.*, 96, article no. 095505.
- Bunde, A. and Havlin, S. (2012). *Fractals and Disordered Systems*. Springer Science & Business Media, Berlin, Heidelberg.
- Byggmästar, J., Hamedani, A., Nordlund, K., and Djurabekova, F. (2019). Machine-learning interatomic potential for radiation damage and defects in tungsten. *Phys. Rev. B*, 100, article no. 144105.
- Car, R. and Parrinello, M. (1985). Unified approach for molecular dynamics and density-functional theory. *Phys. Rev. Lett.*, 55, 2471–2474.
- Car, R. and Parrinello, M. (1988). Structural, dynamical, and electronic properties of amorphous silicon: an ab initio molecular-dynamics study. *Phys. Rev. Lett.*, 60, 204–207.
- Caravati, S., Bernasconi, M., Kühne, T. D., Krack, M., and Parrinello, M. (2009). First-principles study of crystalline and amorphous  $\text{Ge}_2\text{Sb}_2\text{Te}_5$  and the effects of stoichiometric defects. *J. Phys. Condens. Matter*, 21, article no. 255501.
- Caro, M. A. (2019). Optimizing many-body atomic descriptors for enhanced computational performance of machine learning based interatomic potentials. *Phys. Rev. B*, 100, article no. 024112.
- Carré, A., Berthier, L., Horbach, J., Ispas, S., and Kob, W. (2007). Amorphous silica modeled with truncated and screened Coulomb interactions: a molecular dynamics simulation study. *J. Chem. Phys.*, 127, article no. 114512.
- Carré, A., Horbach, J., Ispas, S., and Kob, W. (2008). New fitting scheme to obtain effective potential from Car-Parrinello molecular-dynamics simulations: Application to silica. *Europhys. Lett.*, 82, article no. 17001.
- Carré, A., Ispas, S., Horbach, J., and Kob, W. (2016). Developing empirical potentials from ab initio simulations: the case of amorphous silica. *Comput. Mater. Sci.*, 124, 323–334.
- Chialvo, A. A. and Debenedetti, P. G. (1990). On the use of the Verlet neighbor list in molecular dynamics. *Comput. Phys. Commun.*, 60, 215–224.
- Chmiela, S., Sauceda, H. E., Müller, K.-R., and Tkatchenko, A. (2018). Towards exact molecular dynamics simulations with machine-learned force fields. *Nat. Commun.*, 9, 1–10.
- Christensen, R., Sørensen, S. S., Liu, H., Li, K., Bauchy, M., and Smedskjaer, M. M. (2021). Interatomic potential parameterization using particle swarm optimization: case study of glassy silica. *J. Chem. Phys.*, 154, article no. 134505.
- Cobb, M., Drabold, D. A., and Cappelletti, R. L. (1996). *Ab initio* molecular-dynamics study of the structural, vibrational, and electronic properties of glassy  $\text{GeSe}_2$ . *Phys. Rev. B*, 54, 12162–12171.
- Cormack, A. N. and Du, J. (2001). Molecular dynamics simulations of soda–lime–silicate glasses. *J. Non Cryst. Solids*, 293–295, 283–289. 8th Int. Conf. on Non-Crystalline Materials.
- Cormack, A. N., Du, J., and Zeitler, T. R. (2002). Alkali ion migration mechanisms in silicate glasses probed by molecular dynamics simulations. *Phys. Chem. Chem. Phys.*, 4, 3193–3197.
- Cormier, L., Ghaleb, D., Neuville, D. R., Delaye, J.-M., and Calas, G. (2003). Chemical dependence of network topology of calcium aluminosilicate glasses: a computer simulation study. *J. Non Cryst. Solids*, 332, 255–270.
- Cranmer, M., Sanchez-Gonzalez, A., Battaglia, P., Xu, R., Cranmer, K., Spergel, D., and Ho, S. (2020). Discovering symbolic models from deep learning with inductive biases. In *34th Conference on Neural Information Processing Systems (NeurIPS 2020)*, Vancouver, Canada.
- Cubuk, E. D., Ivancic, R. J. S., Schoenholz, S. S., Strickland, D. J., Basu, A., Davidson, Z. S., Fontaine, J., Hor, J. L., Huang, Y.-R., Jiang, Y., Keim, N. C., Koshigan, K. D., Lefever, J. A., Liu, T., Ma, X.-G., Magagnosc, D. J., Morrow, E., Ortiz, C. P., Rieser, J. M., Shavit, A., Still, T., Xu, Y., Zhang, Y., Nordstrom, K. N., Arratia, P. E., Carpick, R. W., Durian, D. J., Fakhraai, Z., Jerolmack, D. J., Lee, D., Li, J., Riggelman, R., Turner, K. T., Yodh, A. G., Gianola, D. S., and Liu, A. J. (2017). Structure-property relationships from universal signatures of plasticity in disordered solids. *Science*, 358, 1033–1037.
- Darby, J. P., Arhangelskis, M., Katsenis, A. D., Marrett, J. M., Frišćić, T., and Morris, A. J. (2020). Ab initio prediction of metal-organic framework structures. *Chem. Mater.*, 32, 5835–5844.
- Daw, M. S. and Baskes, M. I. (1983). Semiempirical, quantum mechanical calculation of hydrogen embrittlement in metals. *Phys. Rev. Lett.*, 50, 1285–1288.

- Daw, M. S. and Baskes, M. I. (1984). Embedded-atom method: derivation and application to impurities, surfaces, and other defects in metals. *Phys. Rev. B*, 29, 6443–6453.
- Daw, M. S., Foiles, S. M., and Baskes, M. I. (1993). The embedded-atom method: a review of theory and applications. *Mater. Sci. Rep.*, 9, 251–310.
- Debenedetti, P. G. and Stillinger, F. H. (2001). Supercooled liquids and the glass transition. *Nature*, 410, 259–267.
- Deng, L., Miyatani, K., Amma, S., Suehara, M., Ono, M., Yamamoto, Y., Urata, S., and Du, J. (2019). Reaction mechanisms and interfacial behaviors of sodium silicate glass in an aqueous environment from reactive force field-based molecular dynamics simulations. *J. Phys. Chem. C*, 123, 21538–21547.
- Deng, L., Miyatani, K., Suehara, M., Amma, S., Ono, M., Urata, S., and Du, J. (2021). Ion-exchange mechanisms and interfacial reaction kinetics during aqueous corrosion of sodium silicate glasses. *NPJ Mater. Degrad.*, 5, 1–13.
- Deng, L., Urata, S., Takimoto, Y., Miyajima, T., Hahn, S. H., Duin, A. C. T., and van, Du, J. (2020). Structural features of sodium silicate glasses from reactive force field-based molecular dynamics simulations. *J. Am. Ceram. Soc.*, 103, 1600–1614.
- Deringer, V. L., Bernstein, N., Csányi, G., Mahmoud, C. B., Ceriotti, M., Wilson, M., Drabold, D. A., and Elliott, S. R. (2021). Origins of structural and electronic transitions in disordered silicon. *Nature*, 589, 59–64.
- Ding, K. and Andersen, H. C. (1986). Molecular-dynamics simulation of amorphous germanium. *Phys. Rev. B*, 34, 6987–6991.
- Dongol, R., Wang, L., Cormack, A. N., and Sundaram, S. K. (2018). Molecular dynamics simulation of sodium aluminosilicate glass structures and glass surface-water reactions using the reactive force field (ReaxFF). *Appl. Surf. Sci.*, 439, 1103–1110.
- Du, J. (2015). Challenges in molecular dynamics simulations of multicomponent oxide glasses. In Masobrio, C., Du, J., Bernasconi, M., and Salmon, P. S., editors, *Molecular Dynamics Simulations of Disordered Materials: From Network Glasses to Phase-Change Memory Alloys*, Springer Series in Materials Science, pages 157–180. Springer International Publishing, Cham.
- Du, J. (2019). Molecular dynamics simulations of oxide glasses. In Musgraves, J. D., Hu, J., and Calvez, L., editors, *Springer Handbook of Glass*, Springer Handbooks, pages 1131–1155. Springer International Publishing, Cham.
- Du, J. and Cormack, A. N. (2004). The medium range structure of sodium silicate glasses: a molecular dynamics simulation. *J. Non Cryst. Solids*, 349, 66–79. Glass Science for High Technology. 16th University Conference on Glass Science.
- Du, J. and Corrales, L. R. (2006). Compositional dependence of the first sharp diffraction peaks in alkali silicate glasses: A molecular dynamics study. *J. Non Cryst. Solids*, 352, 3255–3269.
- Du, T., Li, H., Sant, G., and Bauchy, M. (2018). New insights into the sol–gel condensation of silica by reactive molecular dynamics simulations. *J. Chem. Phys.*, 148, article no. 234504.
- Du, T., Li, H., Zhou, Q., Wang, Z., Sant, G., Ryan, J. V., and Bauchy, M. (2019a). Atomistic origin of the passivation effect in hydrated silicate glasses. *NPJ Mater. Degrad.*, 3, article no. 6.
- Du, T., Li, H., Zhou, Q., Wang, Z., Sant, G., Ryan, J. V., and Bauchy, M. (2019b). Chemical composition of calcium-silicate-hydrate gels: Competition between kinetics and thermodynamics. *Phys. Rev. Mater.*, 3, article no. 065603.
- Durandurdu, M. and Drabold, D. A. (2002). Simulation of pressure-induced polyamorphism in a chalcogenide glass GeSe<sub>2</sub>. *Phys. Rev. B*, 65, article no. 104208.
- Eckhoff, M. and Behler, J. (2019). From molecular fragments to the bulk: development of a neural network potential for MOF-5. *J. Chem. Theory Comput.*, 15, 3793–3809.
- Erlebach, A., Nachtigall, P., and Grajciar, L. (2021). Accurate large-scale simulations of siliceous zeolites by neural network potentials. [cond-mat.mtrl-sci].
- Ewald, P. (1921). Evaluation of optical and electrostatic lattice potentials. *Ann. Phys.*, 64, 253–287.
- Fennell, C. J. and Gezelter, J. D. (2006). Is the Ewald summation still necessary? Pairwise alternatives to the accepted standard for long-range electrostatics. *J. Chem. Phys.*, 124, article no. 234104.
- Fernandez-Martinez, A., Kalkan, B., Clark, S. M., and Waychunas, G. A. (2013). Pressure-induced polyamorphism and formation of ‘aragonitic’ amorphous calcium carbonate. *Angew. Chem.*, 125, 8512–8515.
- Fischer, H. E., Barnes, A. C., and Salmon, P. S. (2005). Neutron and *x*-ray diffraction studies of liquids and

- glasses. *Rep. Prog. Phys.*, 69, 233–299.
- Fogarty, J. C., Aktulga, H. M., Grama, A. Y., Duin, A. C. T., and van Pandit, S. A. (2010). A reactive molecular dynamics simulation of the silica-water interface. *J. Chem. Phys.*, 132, article no. 174704.
- Frazier, P. I. and Wang, J. (2016). Bayesian optimization for materials design. In *Information Science for Materials Discovery and Design, Springer Series in Materials Science*, pages 45–75. Springer, Cham.
- Friederich, P., Häse, F., Proppe, J., and Aspuru-Guzik, A. (2021). Machine-learned potentials for next-generation matter simulations. *Nat. Mater.*, 20, 750–761.
- Fulde, P. (1995). *Electron Correlations in Molecules and Solids*. Springer Science & Business Media, Berlin, Heidelberg.
- Fullerton, C. J. and Berthier, L. (2020). Glassy behavior of sticky spheres: what lies beyond experimental timescales? *Phys. Rev. Lett.*, 125, article no. 258004.
- Gaillac, R., Pullumbi, P., Beyer, K. A., Chapman, K. W., Keen, D. A., Bennett, T. D., and Coudert, F.-X. (2017). Liquid metal–organic frameworks. *Nat. Mater.*, 16.
- Ganster, P., Benoit, M., Delaye, J.-M., and Kob, W. (2007). Structural and vibrational properties of a calcium aluminosilicate glass: classical force-fields vs. first-principles. *Mol. Simul.*, 33, 1093–1103.
- Ganster, P., Benoit, M., Kob, W., and Delaye, J.-M. (2004). Structural properties of a calcium aluminosilicate glass from molecular-dynamics simulations: A finite size effects study. *J. Chem. Phys.*, 120, 10172–10181.
- Gilmer, J., Schoenholz, S. S., Riley, P. F., Vinyals, O., and Dahl, G. E. (2017). Neural message passing for quantum chemistry. In *International Conference on Machine Learning. Presented at the International Conference on Machine Learning, PMLR, Sydney, Australia*, pages 1263–1272.
- Goldstein, M. (1969). Viscous liquids and the glass transition: a potential energy barrier picture. *J. Chem. Phys.*, 51, 3728–3739.
- Goodwin, A. L., Michel, F. M., Phillips, B. L., Keen, D. A., Dove, M. T., and Reeder, R. J. (2010). Nanoporous structure and medium-range order in synthetic amorphous calcium carbonate. *Chem. Mater.*, 22, 3197–3205.
- Greaves, G. N. and Sen, S. (2007). Inorganic glasses, glass-forming liquids and amorphizing solids. *Adv. Phys.*, 56, 1–166.
- Grigoriev, F. V., Katkova, E. V., Sulimov, A. V., Sulimov, V. B., and Tikhonravov, A. V. (2016). Annealing of deposited SiO<sub>2</sub> thin films: full-atomistic simulation results. *Opt. Mater. Express, OME*, 6, 3960–3966.
- Grimley, D. I., Wright, A. C., and Sinclair, R. N. (1990). Neutron scattering from vitreous silica IV. Time-of-flight diffraction. *J. Non Cryst. Solids*, 119, 49–64.
- Grubmüller, H., Heller, H., Windemuth, A., and Schulten, K. (1991). Generalized verlet algorithm for efficient molecular dynamics simulations with long-range interactions. *Mol. Simul.*, 6, 121–142.
- Gunnarsson, O. and Jones, R. O. (1985). Total-energy differences: sources of error in local-density approximations. *Phys. Rev. B*, 31, 7588–7602.
- Hafner, J. (2008). Ab-initio simulations of materials using VASP: density-functional theory and beyond. *J. Comput. Chem.*, 29, 2044–2078.
- Hamann, D. R., Schlüter, M., and Chiang, C. (1979). Norm-conserving pseudopotentials. *Phys. Rev. Lett.*, 43, 1494–1497.
- Hernandez, A., Balasubramanian, A., Yuan, F., Mason, S. A. M., and Mueller, T. (2019). Fast, accurate, and transferable many-body interatomic potentials by symbolic regression. *NPJ Comput. Mater.*, 5, article no. 112.
- Hockney, R. W. and Eastwood, J. W. (1988). *Computer Simulation Using Particles*. Taylor & Francis Group, New York.
- Hohenberg, P. and Kohn, W. (1964). Inhomogeneous electron gas. *Phys. Rev.*, 136, B864–B871.
- Hoover, W. G. (1985). Canonical dynamics: equilibrium phase-space distributions. *Phys. Rev. A*, 31, 1695–1697.
- Horbach, J., Kob, W., Binder, K., and Angell, C. A. (1996). Finite size effects in simulations of glass dynamics. *Phys. Rev. E*, 54, R5897–R5900.
- Huan, T. D., Batra, R., Chapman, J., Krishnan, S., Chen, L., and Ramprasad, R. (2017). A universal strategy for the creation of machine learning-based atomistic force fields. *NPJ Comput. Mater.*, 3, article no. 37.
- Huang, L. and Kieffer, J. (2015). Challenges in modeling mixed ionic-covalent glass formers. In Masobrio, C., Du, J., Bernasconi, M., and Salmon, P. S., editors, *Molecular Dynamics Simulations of Disordered Materials: From Network Glasses to Phase-Change Memory Alloys, Springer Series in Materials*

- Science*, pages 87–112. Springer International Publishing, Cham.
- Huang, P. Y., Kurasch, S., Alden, J. S., Shekhawat, A., Alemi, A. A., McEuen, P. L., Sethna, J. P., Kaiser, U., and Muller, D. A. (2013). Imaging atomic rearrangements in two-dimensional silica glass: watching Silica's dance. *Science*, 342, 224–227.
- Ispas, S., Benoit, M., Jund, P., and Jullien, R. (2002). Structural properties of glassy and liquid sodium tetrasilicate: comparison between ab initio and classical molecular dynamics simulations. *J. Non Cryst. Solids*, 307–310, 946–955.
- Iype, E., Hütter, M., Jansen, A. P. J., Nedea, S. V., and Rindt, C. C. M. (2013). Parameterization of a reactive force field using a Monte Carlo algorithm. *J. Comput. Chem.*, 34, 1143–1154.
- Jahn, S. and Madden, P. A. (2007). Modeling earth materials from crustal to lower mantle conditions: a transferable set of interaction potentials for the CMAS system. *Phys. Earth Plane. Inter.*, 162, 129–139.
- Jahn, S., Madden, P. A., and Wilson, M. (2006). Transferable interaction model for  $\text{Al}_2\text{O}_3$ . *Phys. Rev. B*, 74, article no. 024112.
- Jain, S. K., Pellenq, R. J.-M., Pkunic, J. P., and Gubbins, K. E. (2006). Molecular modeling of porous carbons using the hybrid reverse Monte Carlo method. *Langmuir*, 22, 9942–9948.
- Johnson, B. G., Gill, P. M. W., and Pople, J. A. (1993). The performance of a family of density functional methods. *J. Chem. Phys.*, 98, 5612–5626.
- Kamitsos, E. I. (2015). Infrared spectroscopy of glasses. In *Modern Glass Characterization*, pages 1–42. John Wiley & Sons, Ltd, Hoboken, NJ.
- Keen, D. A. and McGreevy, R. L. (1990). Structural modelling of glasses using reverse Monte Carlo simulation. *Nature*, 344, 423–425.
- Kieu, L.-H., Delaye, J.-M., Cormier, L., and Stolz, C. (2011). Development of empirical potentials for sodium borosilicate glass systems. *J. Non Cryst. Solids*, 357, 3313–3321.
- Kochkov, D., Smith, J. A., Alieva, A., Wang, Q., Brenner, M. P., and Hoyer, S. (2021). Machine learning accelerated computational fluid dynamics. *Proc. Natl. Acad. Sci. USA*, 118(21), article no. 2101784118.
- Kohn, W. and Sham, L. J. (1965). Self-consistent equations including exchange and correlation effects. *Phys. Rev.*, 140, A1133–A1138.
- Krishnan, N. M. A., Wang, B., Le Pape, Y., Sant, G., and Bauchy, M. (2017b). Irradiation- vs. vitrification-induced disordering: The case of  $\alpha$ -quartz and glassy silica. *J. Chem. Phys.*, 146, article no. 204502.
- Krishnan, N. M. A., Wang, B., Sant, G., Phillips, J. C., and Bauchy, M. (2017c). Revealing the effect of irradiation on cement hydrates: evidence of a topological self-organization. *ACS Appl. Mater. Interfaces*, 9, 32377–32385.
- Krishnan, N. M. A., Wang, B., Yu, Y., Le Pape, Y., Sant, G., and Bauchy, M. (2017a). Enthalpy landscape dictates the irradiation-induced disordering of quartz. *Phys. Rev. X*, 7, article no. 031019.
- Kroeker, S. (2015). Nuclear magnetic resonance spectroscopy of glasses. In *Modern Glass Characterization*, pages 1–30. John Wiley & Sons, Ltd, Hoboken, NJ.
- Lacks, D. J. (2001). Energy landscapes and the non-newtonian viscosity of liquids and glasses. *Phys. Rev. Lett.*, 87, article no. 225502.
- Lacks, D. J. and Osborne, M. J. (2004). Energy landscape picture of overaging and rejuvenation in a sheared glass. *Phys. Rev. Lett.*, 93, article no. 255501.
- Lane, J. M. D. (2015). Cooling rate and stress relaxation in silica melts and glasses via microsecond molecular dynamics. *Phys. Rev. E*, 92, article no. 012320.
- Langreth, D. C. and Mehl, M. J. (1983). Beyond the local-density approximation in calculations of ground-state electronic properties. *Phys. Rev. B*, 28, 1809–1834.
- Le Losq, C., Neuville, D. R., Chen, W., Florian, P., Massiot, D., Zhou, Z., and Greaves, G. N. (2017). Percolation channels: a universal idea to describe the atomic structure and dynamics of glasses and melts. *Sci. Rep.*, 7, article no. 16490.
- Leach, A. R. (2001). *Molecular Modelling: Principles and Applications*. Prentice Hall, New York.
- Levchenko, E. V., Dappe, Y. J., and Ori, G., editors (2020). *Theory and Simulation in Physics for Materials Applications: Cutting-Edge Techniques in Theoretical and Computational Materials Science*, Springer Series in Materials Science. Springer International Publishing, Cham.
- Leven, I., Hao, H., Tan, S., Guan, X., Penrod, K. A., Akbarian, D., Evangelisti, B., Hossain, M. J., Islam, M. M., Koski, J. P., Moore, S., Aktulga, H. M., van Duin, A. C. T., and Head-Gordon, T. (2021). Recent

- advances for improving the accuracy, transferability, and efficiency of reactive force fields. *J. Chem. Theory Comput.*, 17, 3237–3251.
- Levesque, D. and Verlet, L. (1993). Molecular dynamics and time reversibility. *J. Stat. Phys.*, 72, 519–537.
- Li, W. and Ando, Y. (2018). Comparison of different machine learning models for the prediction of forces in copper and silicon dioxide. *Phys. Chem. Chem. Phys.*, 20, 30006–30020.
- Li, X., Song, W., Yang, K., Krishnan, N. M. A., Wang, B., Smedskjaer, M. M., Mauro, J. C., Sant, G., Balonis, M., and Bauchy, M. (2017). Cooling rate effects in sodium silicate glasses: bridging the gap between molecular dynamics simulations and experiments. *J. Chem. Phys.*, 147, article no. 074501.
- Liu, H., Bao, E., Li, E., Cubuk, E. D., Schoenholz, S. S., Xiao, S., Yang, C., Sant, G., Smedskjaer, M. M., and Bauchy, M. (2021b). Finding needles in haystacks: deciphering a structural signature of glass dynamics by machine learning. (under revision).
- Liu, H., Dong, S., Krishnan, N. M. A., Masoero, E., Sant, G., and Bauchy, M. (2019a). Long-term creep deformations in colloidal calcium–silicate–hydrate gels by accelerated aging simulations. *J. Colloid Interface Sci.*, 542, 339–346.
- Liu, H., Dong, S., Tang, L., Krishnan, N. M. A., Sant, G., and Bauchy, M. (2019b). Effects of polydispersity and disorder on the mechanical properties of hydrated silicate gels. *J. Mech. Phys. Solids*, 122, 555–565.
- Liu, H., Fu, Z., Li, Y., Sabri, N. F. A., and Bauchy, M. (2019c). Balance between accuracy and simplicity in empirical forcefields for glass modeling: insights from machine learning. *J. Non Cryst. Solids*, 515, 133–142.
- Liu, H., Fu, Z., Yang, K., Xu, X., and Bauchy, M. (2019d). Machine learning for glass science and engineering: a review. *J. Non Cryst. Solids*, 4, article no. 100036.
- Liu, H., Fu, Z., Yang, K., Xu, X., and Bauchy, M. (2019e). Parameterization of empirical forcefields for glassy silica using machine learning. *MRS Commun.*, 9, 593–599. article no. mrc.2019.47.
- Liu, H., Hahn, S. H., Ren, M., Thiruvillamalai, M., Gross, T. M., Du, J., Duin, A. C. T., and van Kim, S. H. (2020c). Searching for correlations between vibrational spectral features and structural parameters of silicate glass network. *J. Am. Ceram. Soc.*, 103, 3575–3589.
- Liu, H., Huang, Z., Schoenholz, S. S., Cubuk, E. D., Zhao, Z., Chen, R., Smedskjaer, M. M., Sun, Y., Wang, W., and Bauchy, M. (2021a). Bypassing physics laws to simulate complex atom dynamics by observation-based graph networks. (under revision).
- Liu, H., Li, Y., Fu, Z., Li, K., and Bauchy, M. (2020a). Exploring the landscape of Buckingham potentials for silica by machine learning: soft vs hard interatomic forcefields. *J. Chem. Phys.*, 152, article no. 051101.
- Liu, H., Liu, Y., Zhao, Z., Bauchy, M., Schoenholz, S. S., and Cubuk, E. D. (2020b). End-to-End Differentiability and Tensor Processing Unit Computing to Accelerate Materials’ Inverse Design. [https://ml4eng.github.io/camera\\_readys/35.pdf](https://ml4eng.github.io/camera_readys/35.pdf). Presented at the Workshop on machine learning for engineering modeling, simulation and design @ NeurIPS 2020.
- Liu, H., Tang, L., Krishnan, N. M. A., Sant, G., and Bauchy, M. (2019f). Structural percolation controls the precipitation kinetics of colloidal calcium–silicate–hydrate gels. *J. Phys. D: Appl. Phys.*, 52, article no. 315301.
- Liu, H., Xiao, S., Tang, L., Bao, E., Li, E., Yang, C., Zhao, Z., Sant, G., Smedskjaer, M. M., Guo, L., and Bauchy, M. (2021c). Predicting the early-stage creep dynamics of gels from their static structure by machine learning. *Acta Mater.*, 210, article no. 116817.
- Liu, H., Zhang, T., Krishnan, N. M. A., Smedskjaer, M. M., Ryan, J. V., Gin, S., and Bauchy, M. (2019g). Predicting the dissolution kinetics of silicate glasses by topology-informed machine learning. *NPJ Mater. Degrad.*, 3, 1–12.
- Liu, Z., Hu, Y., Li, X., Song, W., Goyal, S., Micoulaut, M., and Bauchy, M. (2018). Glass relaxation and hysteresis of the glass transition by molecular dynamics simulations. *Phys. Rev. B*, 98, article no. 104205.
- Mahadevan, T. S. and Du, J. (2020). Hydration and reaction mechanisms on sodium silicate glass surfaces from molecular dynamics simulations with reactive force fields. *J. Am. Ceram. Soc.*, 103, 3676–3690.
- Mahadevan, T. S. and Du, J. (2021). Atomic and micro-structure features of nanoporous aluminosilicate glasses from reactive molecular dynamics simulations. *J. Am. Ceram. Soc.*, 104, 229–242.
- Martínez, L., Andrade, R., Birgin, E. G., and Martínez,

- J. M. (2009). PACKMOL: a package for building initial configurations for molecular dynamics simulations. *J. Comput. Chem.*, 30, 2157–2164.
- Martyna, G. J., Klein, M. L., and Tuckerman, M. (1992). Nosé–Hoover chains: the canonical ensemble via continuous dynamics. *J. Chem. Phys.*, 97, 2635–2643.
- Martyna, G. J., Tuckerman, M. E., Tobias, D. J., and Klein, M. L. (1996). Explicit reversible integrators for extended systems dynamics. *Mol. Phys.*, 87, 1117–1157.
- Marx, D. and Hutter, J. (2009). *Ab Initio Molecular Dynamics: Basic Theory and Advanced Methods*. Cambridge University Press, New York.
- Massobrio, C., editor (2015). *Molecular Dynamics Simulations of Disordered Materials: From Network Glasses to Phase-Change Memory Alloys*, Springer Series in Materials Science. Springer, Cham, Heidelberg.
- Mauro, J. C. (2018). Decoding the glass genome. Current opinion in solid state and materials science. *Mater. Des. Glasses*, 22, 58–64.
- Mauro, J. C., Tandia, A., Vargheese, K. D., Mauro, Y. Z., and Smedskjaer, M. M. (2016). Accelerating the design of functional glasses through modeling. *Chem. Mater.*, 28, 4267–4277.
- Mauro, J. C. and Varshneya, A. K. (2006). Multiscale modeling of GeSe<sub>2</sub> glass structure. *J. Am. Ceram. Soc.*, 89, 2323–2326.
- Mauro, J. C. and Zanutto, E. D. (2014). Two centuries of glass research: historical trends, current status, and grand challenges for the future. *Int. J. Appl. Glass Sci.*, 5, 313–327.
- McGreevy, R. L. (2001). Reverse Monte Carlo modelling. *J. Phys. Condens. Matter*, 13, R877–R913.
- McGreevy, R. L. and Pusztai, L. (1988). Reverse Monte Carlo simulation: a new technique for the determination of disordered structures. *Mol. Simul.*, 1, 359–367.
- McMillan, P. F., Wilson, M., Daisenberger, D., and Machon, D. (2005). A density-driven phase transition between semiconducting and metallic polyamorphs of silicon. *Nat. Mater.*, 4, 680–684.
- Mead, R. N. and Mountjoy, G. (2006). A molecular dynamics study of the atomic structure of (CaO)<sub>x</sub>(SiO<sub>2</sub>)<sub>1-x</sub> Glasses. *J. Phys. Chem. B*, 110, 14273–14278.
- Micoulaut, M., Kachmar, A., Bauchy, M., Le Roux, S., Massobrio, C., and Boero, M. (2013). Structure, topology, rings, and vibrational and electronic properties of Ge<sub>x</sub>Se<sub>1-x</sub> glasses across the rigidity transition: a numerical study. *Phys. Rev. B*, 88, article no. 054203.
- Micoulaut, M., Vuilleumier, R., and Massobrio, C. (2009). Improved modeling of liquid GeSe<sub>2</sub>: impact of the exchange-correlation functional. *Phys. Rev. B*, 79, article no. 214205.
- Mishin, Y. (2021). Machine-learning interatomic potentials for materials science. *Acta Mater.*, 214, article no. 116980.
- Mocanu, F. C., Konstantinou, K., and Elliott, S. R. (2020). Quench-rate and size-dependent behaviour in glassy Ge<sub>2</sub>Sb<sub>2</sub>Te<sub>5</sub> models simulated with a machine-learned Gaussian approximation potential. *J. Phys. D: Appl. Phys.*, 53, article no. 244002.
- Mocanu, F. C., Konstantinou, K., Lee, T. H., Bernstein, N., Deringer, V. L., Csányi, G., and Elliott, S. R. (2018). Modeling the phase-change memory material, Ge<sub>2</sub>Sb<sub>2</sub>Te<sub>5</sub>, with a machine-learned interatomic potential. *J. Phys. Chem. B*, 122, 8998–9006.
- Mueller, T., Hernandez, A., and Wang, C. (2020). Machine learning for interatomic potential models. *J. Chem. Phys.*, 152, article no. 050902.
- Musgraves, J. D., Hu, J., and Calvez, L., editors (2019). *Springer Handbook of Glass*, Springer Handbooks. Springer International Publishing, Cham.
- Nakamura, T., Hiraoka, Y., Hirata, A., Escolar, E. G., and Nishiura, Y. (2015). Persistent homology and many-body atomic structure for medium-range order in the glass. *Nanotechnology*, 26, article no. 304001.
- Nakano, A., Kalia, R. K., and Vashishta, P. (1994). First sharp diffraction peak and intermediate-range order in amorphous silica: finite-size effects in molecular dynamics simulations. *J. Non Cryst. Solids*, 171, 157–163.
- Nienhuis, E. T., Tuheen, M., Du, J., and McCloy, J. S. (2021). In situ pair distribution function analysis of crystallizing Fe-silicate melts. *J. Mater. Sci.*, 56, 5637–5657.
- Niklasson, A. M. N., Tymczak, C. J., and Challacombe, M. (2006). Time-reversible Born–Oppenheimer molecular dynamics. *Phys. Rev. Lett.*, 97, article no. 123001.
- Noh, J., Gu, G. H., Kim, S., and Jung, Y. (2020). Machine-enabled inverse design of inorganic solid materials: promises and challenges. *Chem. Sci.*, 11, 4871–4881.



- Nosé, S. (1984a). A molecular dynamics method for simulations in the canonical ensemble. *Mol. Phys.*, 52, 255–268.
- Nosé, S. (1984b). A unified formulation of the constant temperature molecular dynamics methods. *J. Chem. Phys.*, 81, 511–519.
- Omelyan, I. P., Mryglod, I. M., and Folk, R. (2002). Optimized verlet-like algorithms for molecular dynamics simulations. *Phys. Rev. E*, 65, article no. 056706.
- Onbaşlı, M. C. and Mauro, J. C. (2020). Modeling of glasses: an overview. In Andreoni, W. and Yip, S., editors, *Handbook of Materials Modeling*, pages 1977–1995. Springer International Publishing, Cham.
- Onbaşlı, M. C., Tandia, A., and Mauro, J. C. (2018). Mechanical and compositional design of high-strength corning gorilla<sup>®</sup> glass. In Andreoni, W. and Yip, S., editors, *Handbook of Materials Modeling: Applications: Current and Emerging Materials*, pages 1–23. Springer International Publishing, Cham.
- Opletal, G., Petersen, T., O'Malley, B., Snook, I., McCulloch, D. G., Marks, N. A., and Yarovsky, I. (2002). Hybrid approach for generating realistic amorphous carbon structure using metropolis and reverse Monte Carlo. *Mol. Simul.*, 28, 927–938.
- Pandey, A., Biswas, P., Bhattarai, B., and Drabold, D. A. (2016a). Realistic inversion of diffraction data for an amorphous solid: the case of amorphous silicon. *Phys. Rev. B*, 94, article no. 235208.
- Pandey, A., Biswas, P., and Drabold, D. A. (2015). Force-enhanced atomic refinement: structural modeling with interatomic forces in a reverse Monte Carlo approach applied to amorphous Si and SiO<sub>2</sub>. *Phys. Rev. B*, 92, article no. 155205.
- Pandey, A., Biswas, P., and Drabold, D. A. (2016b). Inversion of diffraction data for amorphous materials. *Sci. Rep.*, 6, article no. 33731.
- Pandey, K. K., Garg, N., Shanavas, K. V., Sharma, S. M., and Sikka, S. K. (2011). Pressure induced crystallization in amorphous silicon. *J. Appl. Phys.*, 109, article no. 113511.
- Park, C. W., Kornbluth, M., Vandermause, J., Wolverton, C., Kozinsky, B., and Mailoa, J. P. (2021). Accurate and scalable graph neural network force field and molecular dynamics with direct force architecture. *NPJ Comput. Mater.*, 7, 1–9.
- Parr, R. G. (1980). Density functional theory of atoms and molecules. In Fukui, K. and Pullman, B., editors, *Horizons of Quantum Chemistry, Académie Internationale Des Sciences Moléculaires Quantiques/International Academy of Quantum Molecular Science*, pages 5–15. Springer, Netherlands, Dordrecht.
- Pedone, A. (2009). Properties calculations of silica-based glasses by atomistic simulations techniques: a review. *J. Phys. Chem. C*, 113, 20773–20784.
- Pelletier, J.-M. and Qiao, J. (2019). Metallic glasses. In Musgraves, J. D., Hu, J., and Calvez, L., editors, *Springer Handbook of Glass, Springer Handbooks*, pages 617–643. Springer International Publishing, Cham.
- Perdew, J. P., Burke, K., and Ernzerhof, M. (1996a). Generalized gradient approximation made simple. *Phys. Rev. Lett.*, 77, 3865–3868.
- Perdew, J. P., Burke, K., and Wang, Y. (1996b). Generalized gradient approximation for the exchange-correlation hole of a many-electron system. *Phys. Rev. B*, 54, 16533–16539.
- Perdew, J. P. and Zunger, A. (1981). Self-interaction correction to density-functional approximations for many-electron systems. *Phys. Rev. B*, 23, 5048–5079.
- Petri, I., Salmon, P. S., and Fischer, H. E. (2000). Defects in a disordered world: the structure of glassy GeSe<sub>2</sub>. *Phys. Rev. Lett.*, 84, 2413–2416.
- Phillips, J. C. (1979). Topology of covalent non-crystalline solids I: short-range order in chalcogenide alloys. *J. Non Cryst. Solids*, 34, 153–181.
- Phillips, J. C. (1981). Topology of covalent non-crystalline solids II: medium-range order in chalcogenide alloys and ASi(Ge). *J. Non Cryst. Solids*, 43, 37–77.
- Playford, H. Y., Owen, L. R., Levin, I., and Tucker, M. G. (2014). New insights into complex materials using reverse Monte Carlo modeling. *Annu. Rev. Mater. Res.*, 44, 429–449.
- Plimpton, S. (1995a). Computational limits of classical molecular dynamics simulations. *Comput. Mater. Sci.*, 4, 361–364. Proceedings of the Workshop on Glasses and The Glass Transition: 1 Challenges in Materials Theory and Simulation.
- Plimpton, S. (1995b). Fast parallel algorithms for short-range molecular dynamics. *J. Comput. Phys.*, 117, 1–19.
- Pople, J. A., Head-Gordon, M., Fox, D. J., Raghavachari, K., and Curtiss, L. A. (1989).

- Gaussian-1 theory: a general procedure for prediction of molecular energies. *J. Chem. Phys.*, 90, 5622–5629.
- Pun, G. P. P., Batra, R., Ramprasad, R., and Mishin, Y. (2019). Physically informed artificial neural networks for atomistic modeling of materials. *Nat. Commun.*, 10, article no. 2339.
- Rahman, A. and Stillinger, F. H. (1971). Molecular dynamics study of liquid water. *J. Chem. Phys.*, 55, 3336–3359.
- Rappe, A. K. and Goddard, W. A. (1991). Charge equilibration for molecular dynamics simulations. *J. Phys. Chem.*, 95, 3358–3363.
- Rasmussen, C. E. and Williams, C. K. I. (2008). Gaussian processes for machine learning. In *Adaptive Computation and Machine Learning*. MIT Press, Cambridge, MA, 3 print edition.
- Ravinder, R., Sridhara, K. H., Bishnoi, S., Grover, H. S., Bauchy, M., Jayadeva, J., Kodamana, H., and Krishnan, N. M. A. (2020). Deep learning aided rational design of oxide glasses. *Mater. Horiz.*, 7, 1819–1827. article no. D0MH00162G.
- Rimsza, J. M., Deng, L., and Du, J. (2016). Molecular dynamics simulations of nanoporous organosilicate glasses using reactive force field (ReaxFF). *J. Non Cryst. Solids*, 431, 103–111. ISNOG 2014.
- Russell, S. J., Russell, S. J., and Norvig, P. (2010). *Artificial Intelligence: A Modern Approach*. Prentice Hall, Upper Saddle River, NJ.
- Salmon, P. S. and Zeidler, A. (2015). Networks under pressure: the development of *in situ* high-pressure neutron diffraction for glassy and liquid materials. *J. Phys. Condens. Matter*, 27, article no. 133201.
- Sanchez-Lengeling, B. and Aspuru-Guzik, A. (2018). Inverse molecular design using machine learning: generative models for matter engineering. *Science*, 361, 360–365.
- Scherer, C., Schmid, F., Letz, M., and Horbach, J. (2019). Structure and dynamics of B<sub>2</sub>O<sub>3</sub> melts and glasses: from ab initio to classical molecular dynamics simulations. *Comput. Mater. Sci.*, 159, 73–85.
- Schoenholz, S. and Cubuk, E. D. (2020). JAX MD: a framework for differentiable physics. *Adv. Neural Inf. Process. Syst.*, 33, 11428–11441.
- Schütt, K. T., Sauceda, H. E., Kindermans, P.-J., Tkatchenko, A., and Müller, K.-R. (2018). SchNet – a deep learning architecture for molecules and materials. *J. Chem. Phys.*, 148, article no. 241722.
- Senftle, T. P., Hong, S., Islam, M. M., Kylasa, S. B., Zheng, Y., Shin, Y. K., Junkermeier, C., Engel-Herbert, R., Janik, M. J., Aktulga, H. M., Verstraelen, T., Grama, A., and van Duin, A. C. T. (2016). The ReaxFF reactive force-field: development, applications and future directions. *NPJ Comput. Mater.*, 2, 1–14.
- Serva, A., Guerault, A., Ishii, Y., Gouillart, E., Burov, E., and Salanne, M. (2020). Structural and dynamic properties of soda–lime–silica in the liquid phase. *J. Chem. Phys.*, 153, article no. 214505.
- Sheng, H. W., Luo, W. K., Alami, F. M., Bai, J. M., and Ma, E. (2006). Atomic packing and short-to-medium-range order in metallic glasses. *Nature*, 439, 419–425.
- Shewchuk, J. R. (1994). An Introduction to the Conjugate Gradient Method Without the Agonizing Pain. [ftp://ftp.unicauca.edu.co/Facultades/.FIET\\_serepiteencuentasyocupaespacio/DEIC/docs/Materias/computacion%20inteligente/parte%20II/semana12/gradient/painless-conjugate-gradient.pdf](ftp://ftp.unicauca.edu.co/Facultades/.FIET_serepiteencuentasyocupaespacio/DEIC/docs/Materias/computacion%20inteligente/parte%20II/semana12/gradient/painless-conjugate-gradient.pdf).
- Sillar, K., Hofmann, A., and Sauer, J. (2009). Ab Initio study of hydrogen adsorption in MOF-5. *J. Am. Chem. Soc.*, 131, 4143–4150.
- Soper, A. K. (2005). Partial structure factors from disordered materials diffraction data: an approach using empirical potential structure refinement. *Phys. Rev. B*, 72, article no. 104204.
- Sørensen, S. S., Biscio, C. A. N., Bauchy, M., Fajstrup, L., and Smedskjaer, M. M. (2020). Revealing hidden medium-range order in amorphous materials using topological data analysis. *Sci. Adv.*, 6, article no. eabc2320.
- Sosso, G. C., Deringer, V. L., Elliott, S. R., and Csányi, G. (2018). Understanding the thermal properties of amorphous solids using machine-learning-based interatomic potentials. *Mol. Simul.*, 44, 866–880.
- Soules, T. F. (1990). Computer simulation of glass structures. *J. Non Cryst. Solids*, 123, 48–70. XVth International Congress on Glass.
- Steinfeld, J. I., Francisco, J. S., Hase, W. L., and Hase, W. L. (1999). *Chemical Kinetics and Dynamics*. Prentice Hall, Upper Saddle River, NJ.
- Stillinger, F. H. and Rahman, A. (1974). Improved simulation of liquid water by molecular dynamics. *J. Chem. Phys.*, 60, 1545–1557.
- Stillinger, F. H. and Weber, T. A. (1985). Computer

- simulation of local order in condensed phases of silicon. *Phys. Rev. B*, 31, 5262–5271.
- Sundararaman, S., Huang, L., Ispas, S., and Kob, W. (2018). New optimization scheme to obtain interaction potentials for oxide glasses. *J. Chem. Phys.*, 148, article no. 194504.
- Sundararaman, S., Huang, L., Ispas, S., and Kob, W. (2020). New interaction potentials for borate glasses with mixed network formers. *J. Chem. Phys.*, 152, article no. 104501.
- Takada, A. (2021). Atomistic simulations of glass structure and properties. In Richet, P., Conrard, R., Takada, A., and Dyon, J., editors, *Encyclopedia of Glass Science, Technology, History, and Culture*, pages 221–232. Wiley, Hoboken, NJ.
- Tanaka, H., Kawasaki, T., Shintani, H., and Watanabe, K. (2010). Critical-like behaviour of glass-forming liquids. *Nat. Mater.*, 9, 324–331.
- Tanaka, H., Tong, H., Shi, R., and Russo, J. (2019). Revealing key structural features hidden in liquids and glasses. *Nat. Rev. Phys.*, 1, 333–348.
- Tang, L., Liu, H., Ma, G., Du, T., Mousseau, N., Zhou, W., and Bauchy, M. (2021). The energy landscape governs ductility in disordered materials. *Mater. Horiz.*, 8, 1242–1252. article no. DOMH00980F.
- Tanguy, A., Gounelle, M., and Roux, S. (1998). From individual to collective pinning: effect of long-range elastic interactions. *Phys. Rev. E*, 58, 1577–1590.
- Tilocca, A. and de Leeuw, N. H. (2006). Ab initio molecular dynamics study of 45S5 bioactive silicate glass. *J. Phys. Chem. B*, 110, 25810–25816.
- To, T., Sørensen, S. S., Stepniewska, M., Qiao, A., Jensen, L. R., Bauchy, M., Yue, Y., and Smedskjaer, M. M. (2020). Fracture toughness of a metal-organic framework glass. *Nat. Commun.*, 11, article no. 2593.
- Troullier, N. and Martins, J. L. (1991). Efficient pseudopotentials for plane-wave calculations. *Phys. Rev. B*, 43, 1993–2006.
- Tuckerman, M. E., Alejandre, J., López-Rendón, R., Jochim, A. L., and Martyna, G. J. (2006). A Liouville-operator derived measure-preserving integrator for molecular dynamics simulations in the isothermal-isobaric ensemble. *J. Phys. A: Math. Gen.*, 39, 5629–5651.
- Ueno, T., Rhone, T. D., Hou, Z., Mizoguchi, T., and Tsuda, K. (2016). COMBO: an efficient Bayesian optimization library for materials science. *Mater. Discov.*, 4, 18–21.
- Utz, M., Debenedetti, P. G., and Stillinger, F. H. (2000). Atomistic simulation of aging and rejuvenation in glasses. *Phys. Rev. Lett.*, 84, 1471–1474.
- van Beest, B. W. H., Kramer, G. J., and van Santen, R. A. (1990). Force fields for silicas and aluminophosphates based on *ab initio* calculations. *Phys. Rev. Lett.*, 64, 1955–1958.
- van Duin, A. C. T., Dasgupta, S., Lorant, F., and Goddard, W. A. (2001). ReaxFF: a reactive force field for hydrocarbons. *J. Phys. Chem. A*, 105, 9396–9409.
- van Duin, A. C. T., Strachan, A., Stewman, S., Zhang, Q., Xu, X., and Goddard, W. A. (2003). ReaxFF SiO reactive force field for silicon and silicon oxide systems. *J. Phys. Chem. A*, 107, 3803–3811.
- Vanderbilt, D. (1990). Soft self-consistent pseudopotentials in a generalized eigenvalue formalism. *Phys. Rev. B*, 41, 7892–7895.
- Vollmayr, K., Kob, W., and Binder, K. (1996a). Cooling-rate effects in amorphous silica: A computer-simulation study. *Phys. Rev. B*, 54, 15808–15827.
- Vollmayr, K., Kob, W., and Binder, K. (1996b). How do the properties of a glass depend on the cooling rate? A computer simulation study of a Lennard-Jones system. *J. Chem. Phys.*, 105, 4714–4728.
- Vollmayr-Lee, K., Bjorkquist, R., and Chambers, L. M. (2013). Microscopic picture of aging in SiO<sub>2</sub>. *Phys. Rev. Lett.*, 110, article no. 017801.
- Wang, B., Krishnan, N. M. A., Yu, Y., Wang, M., Le Pape, Y., Sant, G., and Bauchy, M. (2017). Irradiation-induced topological transition in SiO<sub>2</sub>: structural signature of networks' rigidity. *J. Non Cryst. Solids*, 463, 25–30.
- Wang, M., Krishnan, N. M. A., Wang, B., Smedskjaer, M. M., Mauro, J. C., and Bauchy, M. (2018). A new transferable interatomic potential for molecular dynamics simulations of borosilicate glasses. *J. Non Cryst. Solids*, 498, 294–304.
- Wang, Y. E., Wei, G.-Y., and Brooks, D. (2019). Benchmarking TPU, GPU, and CPU Platforms for Deep Learning. <https://arxiv.org/abs/1907.10701>. [cs.LG].
- Wang, Z., Du, T., Krishnan, N. M. A., Smedskjaer, M. M., and Bauchy, M. (2020). On the equivalence of vapor-deposited and melt-quenched glasses. *J. Chem. Phys.*, 152, article no. 164504.
- Weigel, C., Cormier, L., Calas, G., Galois, L., and Bowron, D. T. (2008). Intermediate-range order in the silicate network glasses NaFe<sub>x</sub>Al<sub>1-x</sub>Si<sub>2</sub>O<sub>6</sub> ( $x =$

- 0, 0.5, 0.8, 1): a neutron diffraction and empirical potential structure refinement modeling investigation. *Phys. Rev. B*, 78, article no. 064202.
- Welch, R. C., Smith, J. R., Potuzak, M., Guo, X., Bowden, B. F., Kiczinski, T. J., Allan, D. C., King, E. A., Ellison, A. J., and Mauro, J. C. (2013). Dynamics of glass relaxation at room temperature. *Phys. Rev. Lett.*, 110, article no. 265901.
- Wilkinson, C. J. and Mauro, J. C. (2021). Explorer. py: mapping the energy landscapes of complex materials. *SoftwareX*, 14, article no. 100683.
- Wright, A. C. (1988). Neutron and  $x$ -ray amorphography. *J. Non Cryst. Solids*, 106, 1–16.
- Wright, A. C. (1993). The comparison of molecular dynamics simulations with diffraction experiments. *J. Non Cryst. Solids*, 159, 264–268.
- Wright, A. C. (2020). Silicate glass structure: towards a working hypothesis for the 21st century. *Phys. Chem. Glas.*, 61, 57–76.
- Wright, A. C., Clare, A. G., Bachra, B., Sinclair, R. N., Hannon, A. C., and Vessal, B. (1991). Neutron diffraction studies of silicate glasses. In *Proceedings of the Symposium on The Structural Chemistry of Silicates*, pages 239–254, New York, NY, USA. American Crystallographic Assoc.
- Yang, K., Chen, Y.-F., Roumpos, G., Colby, C., and Anderson, J. (2019a). High performance Monte Carlo simulation of ising model on TPU clusters. In *Proceedings of the International Conference for High Performance Computing, Networking, Storage and Analysis. Presented at the SC '19: The International Conference for High Performance Computing, Networking, Storage, and Analysis*, pages 1–15, Denver, Colorado. ACM.
- Yang, K., Xu, X., Yang, B., Cook, B., Ramos, H., Krishnan, N. M. A., Smedskjaer, M. M., Hoover, C., and Bauchy, M. (2019b). Predicting the Young's modulus of silicate glasses using high-throughput molecular dynamics simulations and machine learning. *Sci. Rep.*, 9, 1–11.
- Yang, Y., Shin, Y. K., Li, S., Bennett, T. D., van Duin, A. C. T., and Mauro, J. C. (2018). Enabling computational design of ZIFs using ReaxFF. *J. Phys. Chem. B*, 122, 9616–9624.
- Yang, Y., Zhou, J., Zhu, F., Yuan, Y., Chang, D. J., Kim, D. S., Pham, M., Rana, A., Tian, X., Yao, Y., Osher, S. J., Schmid, A. K., Hu, L., Ercius, P., and Miao, J. (2021). Determining the three-dimensional atomic structure of an amorphous solid. *Nature*, 592, 60–64.
- Yaseen, A., Ji, H., and Li, Y. (2016). A load-balancing workload distribution scheme for three-body interaction computation on Graphics Processing Units (GPU). *J. Parallel Distrib. Comput.*, 87, 91–101.
- Youngman, R. (2018). NMR spectroscopy in glass science: a review of the elements. *Materials*, 11, article no. 476.
- Yu, Y., Krishnan, N. M. A., Smedskjaer, M. M., Sant, G., and Bauchy, M. (2018). The hydrophilic-to-hydrophobic transition in glassy silica is driven by the atomic topology of its surface. *J. Chem. Phys.*, 148, article no. 074503.
- Yu, Y., Wang, B., Wang, M., Sant, G., and Bauchy, M. (2016). Revisiting silica with ReaxFF: towards improved predictions of glass structure and properties via reactive molecular dynamics. *J. Non Cryst. Solids*, 443, 148–154.
- Yu, Y., Wang, B., Wang, M., Sant, G., and Bauchy, M. (2017a). Reactive molecular dynamics simulations of sodium silicate glasses—toward an improved understanding of the structure. *Int. J. Appl. Glass Sci.*, 8, 276–284.
- Yu, Y., Wang, M., Smedskjaer, M. M., Mauro, J. C., Sant, G., and Bauchy, M. (2017b). Thermometer effect: origin of the mixed alkali effect in glass relaxation. *Phys. Rev. Lett.*, 119, article no. 095501.
- Yu, Y., Wang, M., Zhang, D., Wang, B., Sant, G., and Bauchy, M. (2015). Stretched exponential relaxation of glasses at low temperature. *Phys. Rev. Lett.*, 115, article no. 165901.
- Zanotto, E. D. and Coutinho, F. A. B. (2004). How many non-crystalline solids can be made from all the elements of the periodic table? *J. Non Cryst. Solids*, 347, 285–288.
- Zhao, C., Zhou, W., Zhou, Q., Wang, Z., Sant, G., Guo, L., and Bauchy, M. (2021). Topological origin of phase separation in hydrated gels. *J. Colloid Interface Sci.*, 590, 199–209.
- Zhao, C., Zhou, W., Zhou, Q., Zhang, Y., Liu, H., Sant, G., Liu, X., Guo, L., and Bauchy, M. (2020). Precipitation of calcium–alumino–silicate–hydrate gels: the role of the internal stress. *J. Chem. Phys.*, 153, article no. 014501.
- Zhou, Q., Du, T., Guo, L., Smedskjaer, M. M., and Bauchy, M. (2020). New insights into the structure of sodium silicate glasses by force-enhanced atomic refinement. *J. Non Cryst. Solids*, 536, article no. 120006.

Zhou, Q., Shi, Y., Deng, B., Neufeind, J., and Bauchy, M. (2021). Experimental method to quantify the

ring size distribution in silicate glasses and simulation validation thereof. *Sci. Adv.*, 7, article no. eabh1761.